

## ARTICLE

# Foxo1 controls gut homeostasis and commensalism by regulating mucus secretion

Zuojia Chen<sup>1,2</sup>, Jialie Luo<sup>2</sup>, Jian Li<sup>2</sup>, Girak Kim<sup>2</sup>, Eric S. Chen<sup>1</sup>, Sheng Xiao<sup>1</sup>, Scott B. Snapper<sup>4</sup>, Bin Bao<sup>5</sup>, Dingding An<sup>5</sup>, Richard S. Blumberg<sup>6</sup>, Cheng-hui Lin<sup>7</sup>, Sui Wang<sup>7</sup>, Jiixin Zhong<sup>8</sup>, Kuai Liu<sup>8</sup>, Qiyuan Li<sup>8</sup>, Chuan Wu<sup>1,2</sup>, and Vijay K. Kuchroo<sup>1,3</sup>

**Mucus produced by goblet cells in the gastrointestinal tract forms a biological barrier that protects the intestine from invasion by commensals and pathogens. However, the host-derived regulatory network that controls mucus secretion and thereby changes gut microbiota has not been well studied. Here, we identify that Forkhead box protein O1 (Foxo1) regulates mucus secretion by goblet cells and determines intestinal homeostasis. Loss of Foxo1 in intestinal epithelial cells (IECs) results in defects in goblet cell autophagy and mucus secretion, leading to an impaired gut microenvironment and dysbiosis. Subsequently, due to changes in microbiota and disruption in microbiome metabolites of short-chain fatty acids, Foxo1 deficiency results in altered organization of tight junction proteins and enhanced susceptibility to intestinal inflammation. Our study demonstrates that Foxo1 is crucial for IECs to establish commensalism and maintain intestinal barrier integrity by regulating goblet cell function.**

## Introduction

In the gut, the epithelial barrier forms the front line in encountering different environmental insults and protecting host tissues from bacterial invasion. The physical and biochemical barrier functions of the gut epithelium and its associated mucus layer are important not only for colonization of commensal bacteria but also for maintenance of mucosal immune homeostasis. The intestinal epithelium has developed multiple strategies against bacterial adhesion and invasion, including secretion of antimicrobial peptides (AMPs), mucus construction, tight junction (TJ) formation, and innate pathogen sensing (Perez-Lopez et al., 2016; Peterson and Artis, 2014). As one major component of the intestinal barrier, intestinal epithelial cells (IECs) can both sense and respond to external stimuli to maintain barrier integrity. These different methods are reported not only to intrinsically modulate IEC function but also to alter the gut microenvironment, particularly with regard to commensalism.

The gut epithelium regulates the development and colonization of microbiota, and commensal bacteria, in turn, modulate immune responses at mucosal surfaces (Belkaid and Tamoutounour, 2016; Buffie and Pamer, 2013; Marsland and Gollwitzer, 2014). For

instance, it has been reported that enteric IL-17 receptor signaling regulates segmented filamentous bacteria colonization via modulation of AMP production, which in turn influences the development of autoimmunity (Kumar et al., 2016). Similarly, IEC-derived NLRP6 is found to be crucial for clearing enteric pathogens by regulating IL-18 secretion (Elinav et al., 2011). However, the precise molecular mechanisms of how host genes regulate IEC barrier development and function, shaping the gut microbial community and intestinal homeostasis, are not well illustrated.

Goblet cells, a specialized subset of IECs, are mainly responsible for mucin production and secretion (Johansson and Hansson, 2016). The mucus layer, which plays a host-protective role by segregating the microbiota from the intestinal epithelium, is made up predominantly of the highly glycosylated mucin protein Muc2 stored in the secretory granules of goblet cells (Specian and Oliver, 1991; Tytgat et al., 1994). Secretion of mucin from the goblet cells (Artis and Grencis, 2008) is linked to autophagy pathways (Patel et al., 2013; Wlodarska et al., 2014). The secreted mucin proteins form the mucus layer, which in the small intestine is formed of a single layer but in the colon forms a double layer.

<sup>1</sup>Evergrande Center for Immunological Diseases, Harvard Medical School and Brigham and Women's Hospital, Boston, MA; <sup>2</sup>Experimental Immunology Branch, National Cancer Institute, National Institutes of Health, Bethesda, MD; <sup>3</sup>Klarman Cell Observatory, Broad Institute of Massachusetts Institute of Technology and Harvard, Cambridge, MA; <sup>4</sup>Division of Gastroenterology, Hepatology and Nutrition, Boston Children's Hospital, Boston, MA; <sup>5</sup>Department of Pediatrics, Boston Children's Hospital, Boston, MA; <sup>6</sup>Division of Gastroenterology, Hepatology, and Endoscopy, Department of Medicine, Brigham and Women's Hospital, Harvard Medical School, Boston, MA; <sup>7</sup>Department of Ophthalmology, Mary M. and Sash A. Spencer Center for Vision Research, Byers Eye Institute, Stanford University, Stanford, CA; <sup>8</sup>Department of Medicine, School of Medicine, Xiamen University, Xiamen, China.

Correspondence to Chuan Wu: [chuan.wu@nih.gov](mailto:chuan.wu@nih.gov); Vijay K. Kuchroo: [vkuchroo@evergrande.hms.harvard.edu](mailto:vkuchroo@evergrande.hms.harvard.edu); S. Xiao's present address is Celsius Therapeutics, Cambridge, MA.

© 2021 Chen et al. This article is distributed under the terms of an Attribution–Noncommercial–Share Alike–No Mirror Sites license for the first six months after the publication date (see <http://www.rupress.org/terms/>). After six months it is available under a Creative Commons License (Attribution–Noncommercial–Share Alike 4.0 International license, as described at <https://creativecommons.org/licenses/by-nc-sa/4.0/>).

The outer mucus layer of the colon, a loose matrix structure, serves as the habitat for gut microbiota, while the inner mucus layer is firmly associated with epithelium to prevent bacterial invasion, thereby preventing hyperimmune responses to commensal gut microbiota (Johansson and Hansson, 2016; McGuckin et al., 2011; Shan et al., 2013). Loss of Muc2 leads to a disrupted intestinal mucus layer in mice, diminishing the segregation of bacteria from the epithelial cell layer, and increases susceptibility to intestinal inflammation and infection (Gill et al., 2011; Shan et al., 2013; Van der Sluis et al., 2006). While it is clear that goblet cells play a critical role in gut homeostasis, the molecular mechanisms of how goblet cell-derived mucus secretion regulates gut commensalism and intestinal homeostasis are not fully understood.

Forkhead box O (Foxo) proteins have been shown to play important roles in regulating gut dysbiosis and epithelial dysplasia in *Drosophila* (Guo et al., 2014). Foxo transcription factors are also known to be critical for cell survival, cell division, and energy use (Eijkelenboom and Burgering, 2013; Hedrick et al., 2012; van der Horst and Burgering, 2007). We and others previously reported that one of the Foxo family members, Foxo1, plays a critical role in T cell development and function, directing mucosal immune responses and development of intestinal inflammation (Ouyang et al., 2012; Wu et al., 2018a). However, the role of Foxo1 in regulating intestinal barrier function and homeostasis has not been investigated. In this study, we deleted Foxo1 specifically in IECs and demonstrated that Foxo1 plays a critical role in mucin protein secretion by regulating goblet cell autophagy. Loss of Foxo1 in IECs disrupts colonic mucus layer construction, leading to gut microbiome dysbiosis and dysregulated microbial metabolites of short-chain fatty acids (SCFAs). Consequently, Foxo1-deficient mice exhibit impaired intestinal barrier integrity and enhanced susceptibility to gut inflammation. Altogether, our data reveal that IEC-derived Foxo1 shapes intestinal commensalism and epithelial homeostasis by modulating the gut microenvironment of mucus secretion.

## Results

### IEC-derived Foxo1 is critical for intestinal barrier integrity

Within the gastrointestinal tract, Foxo1 was evenly distributed through the intestinal IECs (Fig. S1, A and B). Using an acute colon tissue inflammation model of dextran sulfate sodium (DSS)-induced colitis, we first examined Foxo1 expression in IECs during inflammation and following recovery. We found decreased Foxo1 expression during acute disease development and increased Foxo1 expression during the recovery phase (Fig. 1 A), suggesting a potentially important role of Foxo1 in IEC function. To understand the role of Foxo1 in IECs for intestinal homeostasis and inflammation, we generated IEC-specific Foxo1-deficient mice (*Vil1<sup>Cre</sup>Foxo1<sup>fl/fl</sup>*). Given the known role of Foxo1 in cellular proliferation and apoptosis (Eijkelenboom and Burgering, 2013), we examined the IEC renewal rate and found no defects in IEC proliferation and apoptosis in *Vil1<sup>Cre</sup>Foxo1<sup>fl/fl</sup>* mice (Fig. S1, C and D). We next found that loss of Foxo1 in IECs resulted in more severe DSS-induced colitis than that in *Foxo1<sup>fl/fl</sup>* mice (Fig. 1, B and C). These results suggest that the absence of

Foxo1 selectively in IECs leads to increased susceptibility to intestinal inflammation.

Because one of the major functions of IECs is to maintain epithelial barrier integrity (Peterson and Artis, 2014), we investigated the role of Foxo1 in IECs for intestinal barrier integrity. We discovered that under the steady state, epithelial barrier permeability was significantly increased in *Vil1<sup>Cre</sup>Foxo1<sup>fl/fl</sup>* compared with *Foxo1<sup>fl/fl</sup>* mice (Fig. 1 D). Although *Vil1<sup>Cre</sup>Foxo1<sup>fl/fl</sup>* mice showed normal intestinal tissue morphology when the mice were young (8 wk; Fig. S1 E), they exhibited increased cellular infiltration throughout the intestines as the mice aged (40 wk; Fig. 1, E and F), indicating that the loss of Foxo1 in IECs leads to compromised barrier function and low-grade inflammation in both the small and large intestines. Although TJs are critical for maintaining intestinal epithelial barrier integrity (Turner, 2009), we found no differences in expression of TJ proteins between *Foxo1<sup>fl/fl</sup>* and *Vil1<sup>Cre</sup>Foxo1<sup>fl/fl</sup>* mice (Fig. S1 F). These data suggest that Foxo1 plays an important role in epithelial barrier integrity, which is not due to altered expression of TJ proteins at steady state.

### IEC-derived Foxo1 regulates goblet cell mucus secretion

It is known that Paneth cells are a key IEC subset that is crucial for maintaining epithelial homeostasis and barrier function by limiting bacterial invasion (Adolph et al., 2013; Bel et al., 2017). To first evaluate the role of Foxo1 in Paneth cells in intestinal barrier function, we examined the small intestine and found no abnormal expression of lysozyme or RegIII $\gamma$  in *Vil1<sup>Cre</sup>Foxo1<sup>fl/fl</sup>* mice (Fig. S2, A–C). Moreover, we found no difference in the expression of various AMPs in small intestine IECs between *Foxo1<sup>fl/fl</sup>* and *Vil1<sup>Cre</sup>Foxo1<sup>fl/fl</sup>* mice (Fig. S2 D). We further employed mouse models with a Foxo1 conditional deficiency in Paneth cells (*Defa6<sup>Cre</sup>Foxo1<sup>fl/fl</sup>*; Adolph et al., 2013) and in enteroendocrine cells (*Ngn3<sup>Cre</sup>Foxo1<sup>fl/fl</sup>*). We found no difference in barrier function and DSS-induced colitis between *Foxo1<sup>fl/fl</sup>* and *Defa6<sup>Cre</sup>Foxo1<sup>fl/fl</sup>* or *Ngn3<sup>Cre</sup>Foxo1<sup>fl/fl</sup>* mice, indicating that loss of Foxo1 selectively in Paneth cells or enteroendocrine cells did not affect epithelial barrier function and susceptibility to colitis (Fig. S2, E–H). Additionally, given that *Math1* is known to be critical for goblet cell development (Noah et al., 2011), we generated *Math1<sup>Cre</sup>Foxo1<sup>fl/fl</sup>* mice. *Math1<sup>Cre</sup>Foxo1<sup>fl/fl</sup>* mice exhibited impaired intestinal barrier integrity and enhanced susceptibility to DSS-induced colitis, phenocopying *Vil1<sup>Cre</sup>Foxo1<sup>fl/fl</sup>* mice (Fig. S2, I and J). Since we have ruled out Foxo1's role in other secretory IECs, the phenotype of *Math1<sup>Cre</sup>Foxo1<sup>fl/fl</sup>* mice could be convincingly attributed to goblet cells. We therefore focused our effort back on the *Vil1<sup>Cre</sup>Foxo1<sup>fl/fl</sup>* model, which showed enhanced susceptibility to DSS-induced colitis. To further characterize the intestinal epithelium in the absence of Foxo1, we next examined colonic tissues using periodic acid-Schiff (PAS) staining, which mainly stains the glycosylated proteins in goblet cell mucins. We found that *Vil1<sup>Cre</sup>Foxo1<sup>fl/fl</sup>* mice contained larger areas of cytoplasmic mucin within goblet cells as compared with controls, while the number of goblet cells per crypt was comparable (Fig. 2, A and B). This result was consistent with *Math1<sup>Cre</sup>Foxo1<sup>fl/fl</sup>* mice, confirming that lack of Foxo1 in the intestinal epithelial secretory lineages results in mucus secretion defects (Fig. S2, K

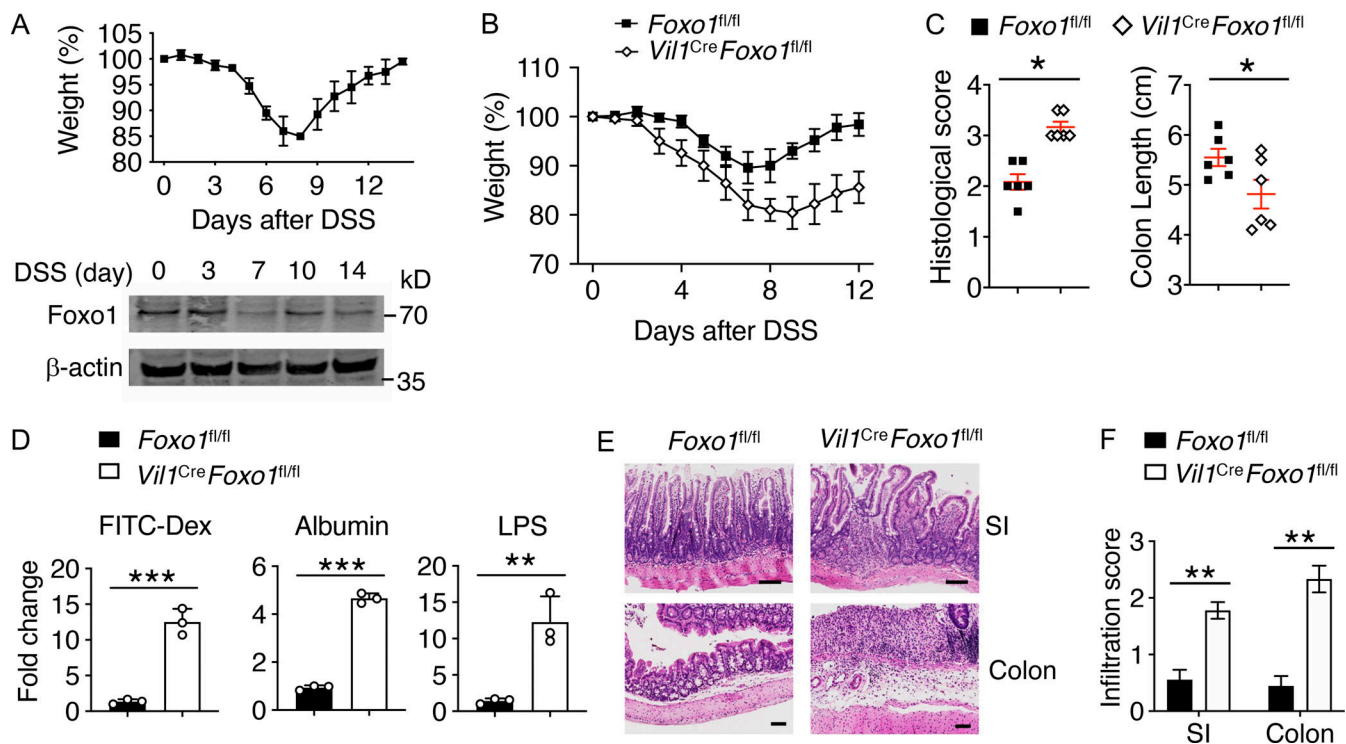


**Figure 1. IEC-derived Foxo1 plays a protective role in colonic homeostasis.** (A) Top: Body weight of WT mice during DSS-induced colitis. Bottom: Immunoblot analysis of Foxo1 protein in colon IECs from WT mice administered DSS at different time points. (B) Body weight of  $Foxo1^{fl/fl}$  and  $Vil1^{Cre}Foxo1^{fl/fl}$  mice during DSS-induced colitis. (C) Histological score (left) and colon lengths (right) of  $Foxo1^{fl/fl}$  and  $Vil1^{Cre}Foxo1^{fl/fl}$  mice during DSS-induced colitis as in B, measured from the colocolic junction to the anal verge. (D) Intestinal barrier permeability was assessed by serum FITC-dextran (FITC-Dex) fluorescence, fecal albumin concentration, and LPS levels in mesenteric LNs from  $Foxo1^{fl/fl}$  and  $Vil1^{Cre}Foxo1^{fl/fl}$  mice. (E) H&E staining of sections of the small intestine (SI) and colon of 40-wk-old  $Foxo1^{fl/fl}$  and  $Vil1^{Cre}Foxo1^{fl/fl}$  mice. Scale bar, 100  $\mu$ m. (F) Quantification of the histological analysis in the SI and colon for mice 40 wk of age on a scale of 0 (no mononuclear infiltration) to 3 (considerable mononuclear infiltration). Data are representative of three independent experiments (A, D, and E) or are pooled from two independent experiments (B, C, and F). \*,  $P < 0.05$ ; \*\*,  $P < 0.01$ ; \*\*\*,  $P < 0.001$  (Student's *t* test; error bars represent SD).

and L). Whole-mount colonic tissue analysis stained with *Ulex europaeus* agglutinin I (UEA) also revealed larger mucin granules in  $Vil1^{Cre}Foxo1^{fl/fl}$  mice (Fig. 2 C). Interestingly, although it is a signature gene of goblet cells, *Muc2* showed no differences in mRNA expression between  $Foxo1^{fl/fl}$  and  $Vil1^{Cre}Foxo1^{fl/fl}$  mice (Fig. 2 D). There were also no significant changes in expression of other key genes for goblet cell development and differentiation between  $Foxo1^{fl/fl}$  and  $Vil1^{Cre}Foxo1^{fl/fl}$  IECs (Fig. 2 E). It is known that goblet cells are mainly responsible for mucin protein secretion and mucus layer construction in the lumen of the gastrointestinal tract (Johansson and Hansson, 2016). Using transmission electron microscopy (TEM), we found that  $Vil1^{Cre}Foxo1^{fl/fl}$  goblet cells contained significantly larger mucin granules than did  $Foxo1^{fl/fl}$  controls (Fig. 2, F and G). Given the normal levels of *Muc2* expression and the increased accumulation of intracellular mucin granules in  $Vil1^{Cre}Foxo1^{fl/fl}$  IECs, we hypothesized that there might be a mucus secretion defect in goblet cells in the absence of Foxo1, which may in turn affect the formation of the mucus layer. Indeed, by performing bacterial 16S rDNA fluorescence in situ hybridization (FISH), we found that  $Vil1^{Cre}Foxo1^{fl/fl}$  mice lack a thick, continuous, overlaying inner mucus layer in the colon (Fig. 2, H and I, dotted line is the inner mucus layer). Additionally, we generated goblet cell-enriched colonic organoids (Patel et al., 2013) and found

enhanced mucin accumulation in  $Vil1^{Cre}Foxo1^{fl/fl}$  organoids compared with controls without altering *Muc2* expression (Fig. S2, M–O). These results indicate the intrinsic effect of Foxo1 for the goblet cell function of mucin secretion.

#### Cytosolic Foxo1 regulates mucus secretion via autophagy

To investigate the molecular mechanisms of how Foxo1 regulates epithelial barrier function, we performed mRNA sequencing of  $Foxo1^{fl/fl}$  and  $Vil1^{Cre}Foxo1^{fl/fl}$  colonic IECs isolated from naive mice. We reanalyzed published microarray data of regulatory T (T reg) cells from  $Foxp3^{Cre}Foxo1^{fl/fl}$  mice (Ouyang et al., 2012) and compared them with our mRNA-sequencing (mRNA-seq) data from IECs. We noticed that while WT and Foxo1-deficient T reg cells exhibited markedly different mRNA expression,  $Foxo1^{fl/fl}$  and  $Vil1^{Cre}Foxo1^{fl/fl}$  IECs under steady state had nearly identical mRNA profiles (Fig. 3 A). These results suggest that, under steady state, Foxo1 does not regulate IEC function by affecting transcription. Indeed, instead of Foxo1 localizing in the nucleus as in naive CD4<sup>+</sup> T cells (Ouyang et al., 2012), we found that Foxo1 mostly localized in the cytoplasm of IECs (Fig. S3 A and Fig. 3 B). More important, quantitative studies confirmed it was goblet cells that mainly expressed cytosolic Foxo1 (Fig. 3, C and D; and Fig. S3 B). These data suggest that Foxo1 may use alternative mechanisms other than transcriptional regulation to control goblet cell function.

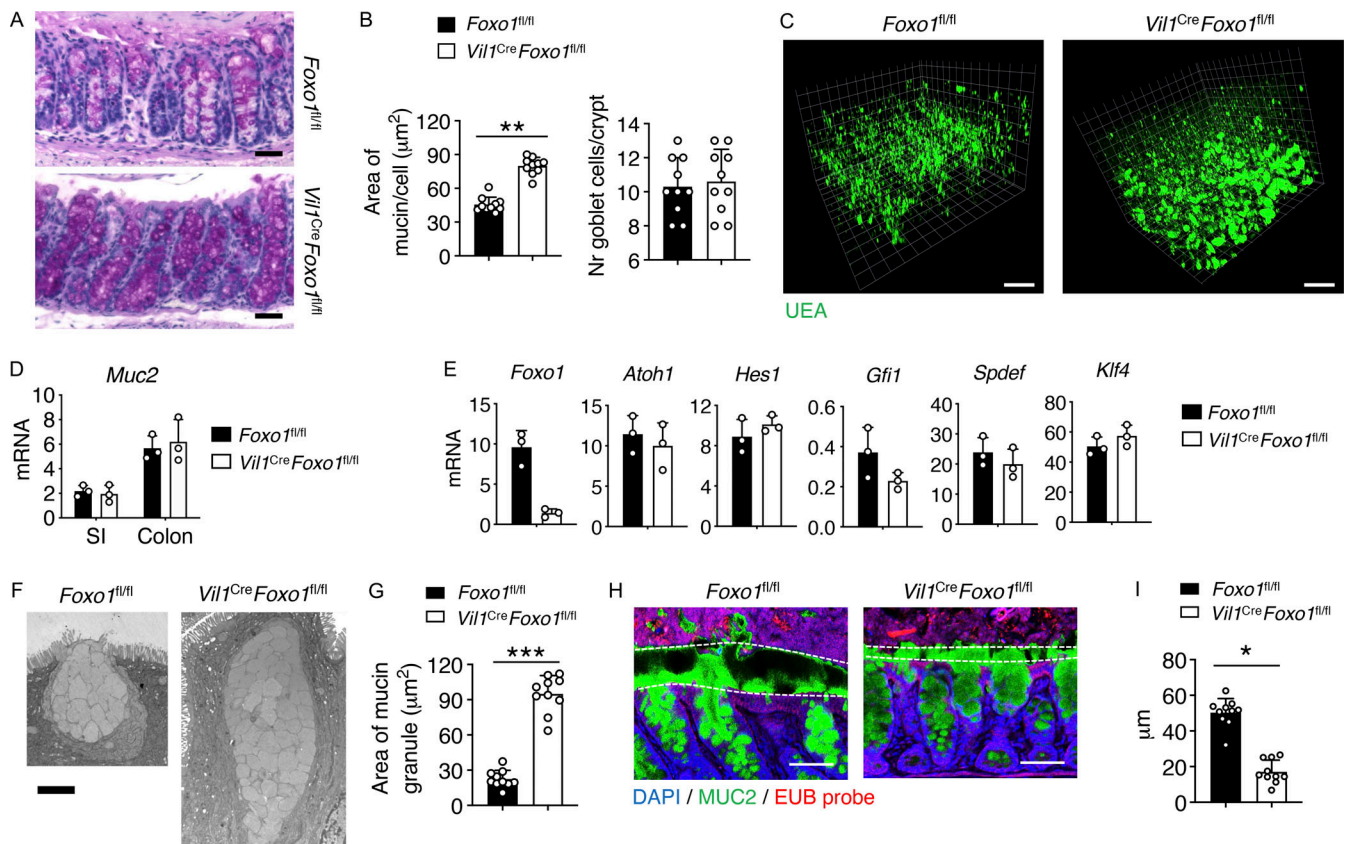


**Figure 2. Foxo1 regulates colonic goblet cell function of mucin secretion.** (A) PAS staining of colons from 8-wk-old *Foxo1<sup>fl/fl</sup>* and *Vil1<sup>Cre</sup>Foxo1<sup>fl/fl</sup>* mice. Scale bar, 100  $\mu$ m. (B) Quantification of the average mucin area/goblet cell (left) and quantification of the average number of goblet cells per crypt (right) in *Foxo1<sup>fl/fl</sup>* and *Vil1<sup>Cre</sup>Foxo1<sup>fl/fl</sup>* mice from A. >100 crypts per mouse were measured. (C) Immunolabeling-enabled three-dimensional imaging of solvent-cleared organs staining from the colonic tissues stained with UEA isolated from *Foxo1<sup>fl/fl</sup>* and *Vil1<sup>Cre</sup>Foxo1<sup>fl/fl</sup>* mice. Scale bar, 50  $\mu$ m. (D) qPCR analysis of *Muc2* mRNA in IECs isolated from the small intestine (SI) and colon of *Foxo1<sup>fl/fl</sup>* and *Vil1<sup>Cre</sup>Foxo1<sup>fl/fl</sup>* mice. (E) qPCR analysis of the indicated genes in IECs from the colons of *Foxo1<sup>fl/fl</sup>* and *Vil1<sup>Cre</sup>Foxo1<sup>fl/fl</sup>* mice. (F) TEM images of upper crypt goblet cells from *Foxo1<sup>fl/fl</sup>* and *Vil1<sup>Cre</sup>Foxo1<sup>fl/fl</sup>* murine colons. Scale bar, 2  $\mu$ m. (G) Quantification of average mucin granule area from F. (H) Representative immunofluorescence staining for mucus of colons from *Foxo1<sup>fl/fl</sup>* and *Vil1<sup>Cre</sup>Foxo1<sup>fl/fl</sup>* mice using MUC2 (green) and EUB338 (EUB) probe (red) with DAPI (blue). The white dashed lines outline the inner mucus layer. Scale bar, 50  $\mu$ m. (I) Quantification of inner mucus layer thickness in the colon as in H (>10 fields measured per mouse). Data are representative of three independent experiments (A, C, F, and H) or are pooled from two independent experiments (B, D, E, G, and I). \*,  $P < 0.05$ ; \*\*,  $P < 0.01$ ; \*\*\*,  $P < 0.001$  (Student's *t* test; error bars represent SD).

Cytosolic Foxo1 has been reported to be essential for the induction of autophagy during tumor suppression via interactions with the autophagy factor ATG7 (Zhao et al., 2010). Autophagy has been linked to the goblet cell function of mucus secretion, raising the question whether loss of Foxo1 affects the process of autophagy in goblet cells (Patel et al., 2013). Although ATG5 and ATG7 protein levels were not altered, the autophagy marker LC3-II was reduced in IECs from the colon of *Vil1<sup>Cre</sup>Foxo1<sup>fl/fl</sup>* mice compared with *Foxo1<sup>fl/fl</sup>* mice (Fig. 3 E). We also found protein-protein interactions between Foxo1 and ATG5 but not ATG7 in IECs (Fig. 3 F). Because ATG5 is known to control goblet cell mucus secretion via the production of ROS (Patel et al., 2013), we hypothesized that interaction between Foxo1 and ATG5 promoted ROS generation. Indeed, we observed less ROS production from colonic IECs of *Vil1<sup>Cre</sup>Foxo1<sup>fl/fl</sup>* mice than from those of *Foxo1<sup>fl/fl</sup>* mice (Fig. 3, G and H), indicating that Foxo1 is required for ATG5 to promote autophagy and mucin secretion in goblet cells.

To further characterize the role of cytosolic Foxo1 in epithelial barrier function, we employed a mouse strain expressing

a mutant form of Foxo1 that is refractory to Akt-targeted inhibition (*Rosa26-fllox-STOP-Foxo1<sup>AAA</sup>*; *Foxo1<sup>AAA</sup>*; Ouyang et al., 2012). Upon breeding the *Foxo1<sup>AAA</sup>* allele to *Vil1<sup>Cre</sup>Foxo1<sup>fl/fl</sup>* mice, we were able to restore Foxo1 expression while restricting it within the IEC nucleus (Fig. S3 C). Interestingly, despite the restored Foxo1 expression, *Vil1<sup>Cre</sup>Foxo1<sup>fl/fl</sup>Foxo1<sup>AAA/+</sup>* mice exhibited larger areas of cytoplasmic mucin within goblet cells than did *Foxo1<sup>fl/fl</sup>* mice (Fig. S3, D and E), as well as more accumulated mucin granules (Fig. S3, F and G). Similar to *Vil1<sup>Cre</sup>Foxo1<sup>fl/fl</sup>* mice, *Vil1<sup>Cre</sup>Foxo1<sup>fl/fl</sup>Foxo1<sup>AAA/+</sup>* mice showed a thinner inner mucus layer than seen in *Foxo1<sup>fl/fl</sup>* control mice (Fig. 3, I and J). We also noticed that IECs from *Vil1<sup>Cre</sup>Foxo1<sup>fl/fl</sup>Foxo1<sup>AAA/+</sup>* mice showed less ROS generation than IECs in *Foxo1<sup>fl/fl</sup>* mice (Fig. S3, H and I). Functionally, we observed compromised barrier integrity and severe DSS-induced colitis in *Vil1<sup>Cre</sup>Foxo1<sup>fl/fl</sup>Foxo1<sup>AAA/+</sup>* mice compared with *Foxo1<sup>fl/fl</sup>* mice (Fig. 3, K and L; and Fig. S3 J). By using *Foxo1<sup>AAA</sup>* mice, we show that, regardless of restored Foxo1 expression, nuclear Foxo1 is dispensable for goblet cell mucin secretion,

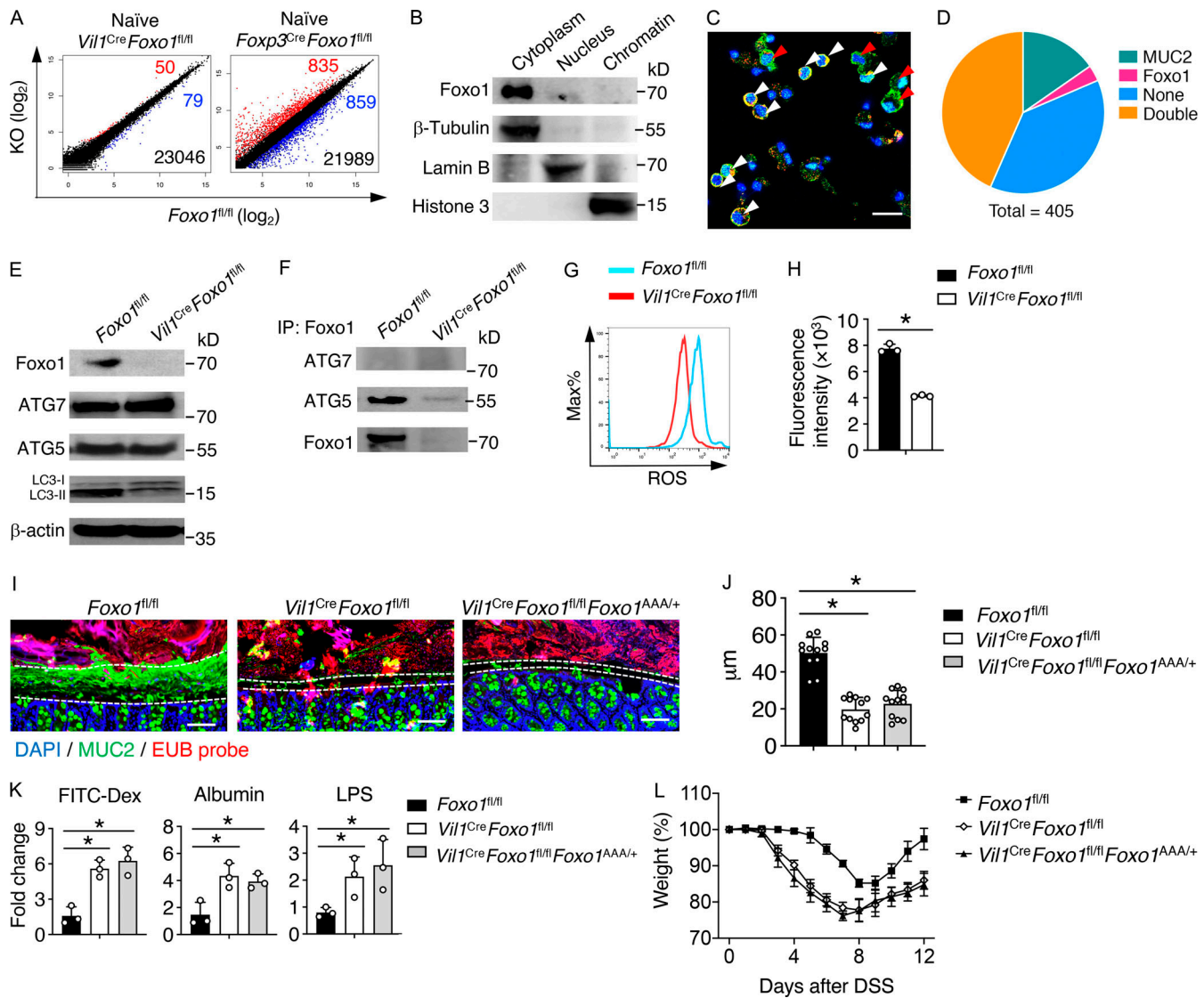


**Figure 3. Cytosolic Foxo1 regulates autophagy in IECs. (A)** Left: RNA-seq analysis of *Foxo1<sup>fl/fl</sup>* and *Vil1<sup>Cre</sup>Foxo1<sup>fl/fl</sup>* mice colonic IECs under steady state. Right: Microarray analysis of *Foxo1<sup>fl/fl</sup>* and *Foxp3<sup>Cre</sup>Foxo1<sup>fl/fl</sup>* mice natural T reg cells under steady state (Gene Expression Omnibus accession no. GSE40657). WT-specific sites (blue) and KO-specific sites (red). Log<sub>2</sub> fold change >1 and P < 0.05. **(B)** Immunoblot analysis of Foxo1, β-tubulin, lamin B, and β-actin in WT colonic IECs. **(C)** Foxo1 (red), MUC2 (green), and DAPI (blue) staining of WT colonic IECs. Red arrowhead: MUC2 single positive; white arrowhead: MUC2 and Foxo1 double positive. Scale bar, 500 μm. **(D)** Quantitative analysis of Foxo1 colocalization with MUC2 in colonic IECs. MUC2, Muc2 single-positive cells; Foxo1, Foxo1 single-positive cells; None, DAPI single-positive cells; Double, MUC2 and Foxo1 double-positive cells. **(E)** Immunoblot analysis of Foxo1, ATG7, ATG5, LC3, and β-actin in colonic IECs from *Foxo1<sup>fl/fl</sup>* and *Vil1<sup>Cre</sup>Foxo1<sup>fl/fl</sup>* mice. **(F)** Coimmunoprecipitation (IP) with antibody to Foxo1 of proteins from *Foxo1<sup>fl/fl</sup>* and *Vil1<sup>Cre</sup>Foxo1<sup>fl/fl</sup>* murine colonic IECs detected by immunoblot analysis (IB) with anti-ATG7, anti-ATG5, or anti-Foxo1. **(G)** Expression of ROS (DCFDA) in *Foxo1<sup>fl/fl</sup>* and *Vil1<sup>Cre</sup>Foxo1<sup>fl/fl</sup>* colonic IECs assessed by flow cytometry. **(H)** Expression of ROS (DCFDA) in *Foxo1<sup>fl/fl</sup>* and *Vil1<sup>Cre</sup>Foxo1<sup>fl/fl</sup>* colonic IECs assessed by fluorescent plate reader. **(I)** Representative immunofluorescence staining for mucus of the colons from *Foxo1<sup>fl/fl</sup>*, *Vil1<sup>Cre</sup>Foxo1<sup>fl/fl</sup>*, and *Vil1<sup>Cre</sup>Foxo1<sup>fl/fl</sup>Foxo1<sup>AAA/+</sup>* mice using MUC2 (green) and EUB338 probe (red) with DAPI (blue). The white dashed lines outline the inner mucus layer. Scale bar, 50 μm. **(J)** Quantification of inner mucus layer thickness in the colon as in I (>10 fields measured per mouse). **(K)** Intestinal barrier permeability was assessed by FITC-dextran (FITC-Dex), albumin, and LPS assays between *Foxo1<sup>fl/fl</sup>*, *Vil1<sup>Cre</sup>Foxo1<sup>fl/fl</sup>*, and *Vil1<sup>Cre</sup>Foxo1<sup>fl/fl</sup>Foxo1<sup>AAA/+</sup>* mice. **(L)** Body weights of *Foxo1<sup>fl/fl</sup>*, *Vil1<sup>Cre</sup>Foxo1<sup>fl/fl</sup>*, and *Vil1<sup>Cre</sup>Foxo1<sup>fl/fl</sup>Foxo1<sup>AAA/+</sup>* mice during DSS-induced colitis. Data are representative of three independent experiments (A–C, E–I, and K) or are pooled from two independent experiments (D, J, and L). \*, P < 0.05 (Student’s t test; error bars represent SD).

demonstrating the importance of cytoplasmic Foxo1 in maintaining IEC homeostasis.

**IEC-derived Foxo1 regulates intestinal barrier integrity via gut microbiota**

It has been shown that IECs and microbiota reciprocally regulate each other in order to maintain intestinal homeostasis and

control inflammation (Buffie and Pamer, 2013; Perez-Lopez et al., 2016; Peterson and Artis, 2014). To determine whether Foxo1 modulates intestinal barrier function intrinsically via goblet cells or extrinsically via gut microbiota, we examined intestinal barrier function in *Foxo1<sup>fl/fl</sup>* and *Vil1<sup>Cre</sup>Foxo1<sup>fl/fl</sup>* mice under either separated housing or cohousing conditions. We used *Vil1<sup>Cre</sup>Foxo1<sup>fl/+</sup>* and *Foxo1<sup>fl/fl</sup>* as breeders and used their

offspring of *Vil1<sup>Cre</sup>Foxo1<sup>fl/fl</sup>* and *Foxo1<sup>fl/fl</sup>* for our experiments. For cohousing experiments, 4-wk-old mice originating from the same breeders were divided to be either housed singly or cohoused with age- and sex-matched mice for 6 wk. To our surprise, after 6 wk of cohousing, while barrier function in *Vil1<sup>Cre</sup>Foxo1<sup>fl/fl</sup>* mice remained the same as that of mice in the separated housing condition, we observed elevated barrier permeability in *Foxo1<sup>fl/fl</sup>* mice compared to *Vil1<sup>Cre</sup>Foxo1<sup>fl/fl</sup>* mice (Fig. 4 A). Furthermore, we found that cohoused *Foxo1<sup>fl/fl</sup>* mice exhibited enhanced susceptibility to DSS-induced colitis, similar to that in *Vil1<sup>Cre</sup>Foxo1<sup>fl/fl</sup>* mice, as compared with *Foxo1<sup>fl/fl</sup>* separated mice (Fig. 4 B and Fig. S4 A), suggesting that impaired intestinal barrier function and enhanced colitis in *Vil1<sup>Cre</sup>Foxo1<sup>fl/fl</sup>* mice may be microbiota dependent. We also found that under the cohousing condition, *Vil1<sup>Cre</sup>Foxo1<sup>fl/fl</sup>* mice still exhibited larger areas of cytoplasmic mucin within goblet cells compared with cohoused *Foxo1<sup>fl/fl</sup>* mice (Fig. S4, B and C). Moreover, cohousing did not alter the mucin granule accumulation in either *Foxo1<sup>fl/fl</sup>* or *Vil1<sup>Cre</sup>Foxo1<sup>fl/fl</sup>* goblet cells compared with the separated housing condition (Fig. 4, C and D), indicating that microbiota did not impact the cell-intrinsic effect of Foxo1. We then found diminished host-microbiota segregation in *Vil1<sup>Cre</sup>Foxo1<sup>fl/fl</sup>* mice compared with *Foxo1<sup>fl/fl</sup>* mice under separated housing conditions. A similar reduced segregation was also observed in *Foxo1<sup>fl/fl</sup>* mice when they were cohoused with *Vil1<sup>Cre</sup>Foxo1<sup>fl/fl</sup>* mice (Fig. S4, D and E). Consistent with this observation, we found thinner mucus layers in the colons of both cohoused *Foxo1<sup>fl/fl</sup>* and *Vil1<sup>Cre</sup>Foxo1<sup>fl/fl</sup>* mice than in separately housed mice (Fig. 4, E and F), indicating that barrier integrity in *Vil1<sup>Cre</sup>Foxo1<sup>fl/fl</sup>* mice is compromised due to dysbiosis caused by altered goblet cell function.

Then, we asked why cohousing reduced the *Foxo1<sup>fl/fl</sup>* colon mucus thickness. It has been reported that gut microbiota uses mucinase to digest glycoproteins from the mucus layer to obtain nutrition (Desai et al., 2016; Marcobal et al., 2013). Additionally, dysbiosis has been reported to induce dysregulated mucus consumption (Desai et al., 2016). Indeed, we found that fecal microbiota from separately housed *Vil1<sup>Cre</sup>Foxo1<sup>fl/fl</sup>* mice exhibited markedly enhanced mucus digestive activity compared with those from *Foxo1<sup>fl/fl</sup>* mice. Using fecal bacteria grown on *Brucella* plates containing 0.5% bovine submaxillary mucin followed by amido black staining (Nesta et al., 2014), we found reduced mucin protein abundance after culturing with fecal microbiota from separately housed *Vil1<sup>Cre</sup>Foxo1<sup>fl/fl</sup>* mice, suggesting enhanced mucus digestive activity as compared with fecal microbiota from *Foxo1<sup>fl/fl</sup>* mice. Furthermore, cohousing resulted in bacteria with elevated mucinase activity within the *Foxo1<sup>fl/fl</sup>* feces (Fig. 4 G). Next, we rederived *Foxo1<sup>fl/fl</sup>* and *Vil1<sup>Cre</sup>Foxo1<sup>fl/fl</sup>* mice in germ-free (GF) conditions to eliminate the effects of the microbiota. Similarly to the specific pathogen-free mice (Fig. 2), we found greater areas of cytoplasmic mucin within goblet cells in GF *Vil1<sup>Cre</sup>Foxo1<sup>fl/fl</sup>* mice than GF WT mice by PAS staining (Fig. 4, H and I). TEM revealed that GF *Vil1<sup>Cre</sup>Foxo1<sup>fl/fl</sup>* goblet cells also contained significantly larger mucin granules than those in controls (Fig. 4, J and K). These data indicate the intrinsic effect of Foxo1 for mucus secretion. Importantly, we found equal levels of epithelial permeability in GF *Foxo1<sup>fl/fl</sup>* and *Vil1<sup>Cre</sup>Foxo1<sup>fl/fl</sup>* mice (Fig. 4 L), suggesting that the

gut microbiota but not mucus secretion determines intestinal barrier function. Therefore, altered gut microbiota is responsible for enhanced susceptibility to DSS in *Vil1<sup>Cre</sup>Foxo1<sup>fl/fl</sup>* mice.

### IEC-derived Foxo1 governs bidirectional regulation of mucus and the gut microbiota

To further understand the role of the microbiota in Foxo1-mediated epithelial homeostasis, we performed microbiota transfer studies in GF host mice. We first reconstituted GF mice with either *Foxo1<sup>fl/fl</sup>* or *Vil1<sup>Cre</sup>Foxo1<sup>fl/fl</sup>* gut microbiota by fecal transplant (Fig. 5 A). We found that in the GF host, *Vil1<sup>Cre</sup>Foxo1<sup>fl/fl</sup>* microbiota reconstitution resulted in a thinner mucus layer than seen after reconstitution with *Foxo1<sup>fl/fl</sup>* microbiota (Fig. 5, B and C), consistent with the in vitro data (Fig. 4 G). As a consequence, GF mice with *Vil1<sup>Cre</sup>Foxo1<sup>fl/fl</sup>* bacteria reconstitution exhibited enhanced intestinal barrier permeability and more severe colitis than those reconstituted with *Foxo1<sup>fl/fl</sup>* mouse bacteria (Fig. 5, D and E; and Fig. S4 F). We next pretreated *Vil1<sup>Cre</sup>Foxo1<sup>fl/fl</sup>* mice with an antibiotic cocktail and then supplemented these mice with gavaged mucin (Fig. 5 F). After mucin protein treatment, we observed enhanced mucus thickness compared with control treatment (Fig. S4, G and H). We also found that mucin treatment did, in fact, modify the gut microbiota composition (Fig. S4 I) and reduced levels of mucinase active bacteria, which were previously identified as having the ability to produce mucin-degrading enzymes targeting a wide range of mucin carbohydrates (Bell et al., 2019; Hoskins et al., 1997; Katayama et al., 2005; Fig. S4 J; and Fig. 5 G). In fact, *Vil1<sup>Cre</sup>Foxo1<sup>fl/fl</sup>* mice that were administered supplementary mucus exhibited improved barrier function and attenuated DSS-induced colitis compared with PBS-treated mice (Fig. 5, H and I; and Fig. S4 K). We concluded that in *Vil1<sup>Cre</sup>Foxo1<sup>fl/fl</sup>* mice, mucin treatment-derived concurrent mucus layer and microbiota changes resulted in reduced sensitivity to DSS-induced colitis. Altogether, our results indicate that Foxo1 is required for the secretion of mucus and the formation of a functional mucus layer, which then contributes to defining the commensal organisms. Consequently, the reciprocal regulation between the mucus and the gut microbiota determines intestinal barrier integrity.

### IEC-derived Foxo1 deficiency results in colonic dysbiosis

To better understand the mechanisms of how the microbiota alter epithelial barrier function and inflammation susceptibility in *Vil1<sup>Cre</sup>Foxo1<sup>fl/fl</sup>* mice, we examined fecal bacteria in *Foxo1<sup>fl/fl</sup>* and *Vil1<sup>Cre</sup>Foxo1<sup>fl/fl</sup>* mice under either separate housing or cohousing conditions. From fecal samples of *Foxo1<sup>fl/fl</sup>* and *Vil1<sup>Cre</sup>Foxo1<sup>fl/fl</sup>* mice before and after weaning, we noticed clear microbiota divergence related to mouse development and separation, suggesting that the host gene of Foxo1 determines microbiota development (Fig. 6 A). 16S rDNA sequence analysis showed that adult *Foxo1<sup>fl/fl</sup>* mice harbored a microbiome with a different community composition and less diversity as compared with *Vil1<sup>Cre</sup>Foxo1<sup>fl/fl</sup>* mice in separate housing (Fig. 6, B and C). Additionally, after 6 wk of cohousing, the microbial composition of both *Foxo1<sup>fl/fl</sup>* and *Vil1<sup>Cre</sup>Foxo1<sup>fl/fl</sup>* mice became similar to the composition of separately housed *Vil1<sup>Cre</sup>Foxo1<sup>fl/fl</sup>* mice (Fig. 6, B and C).

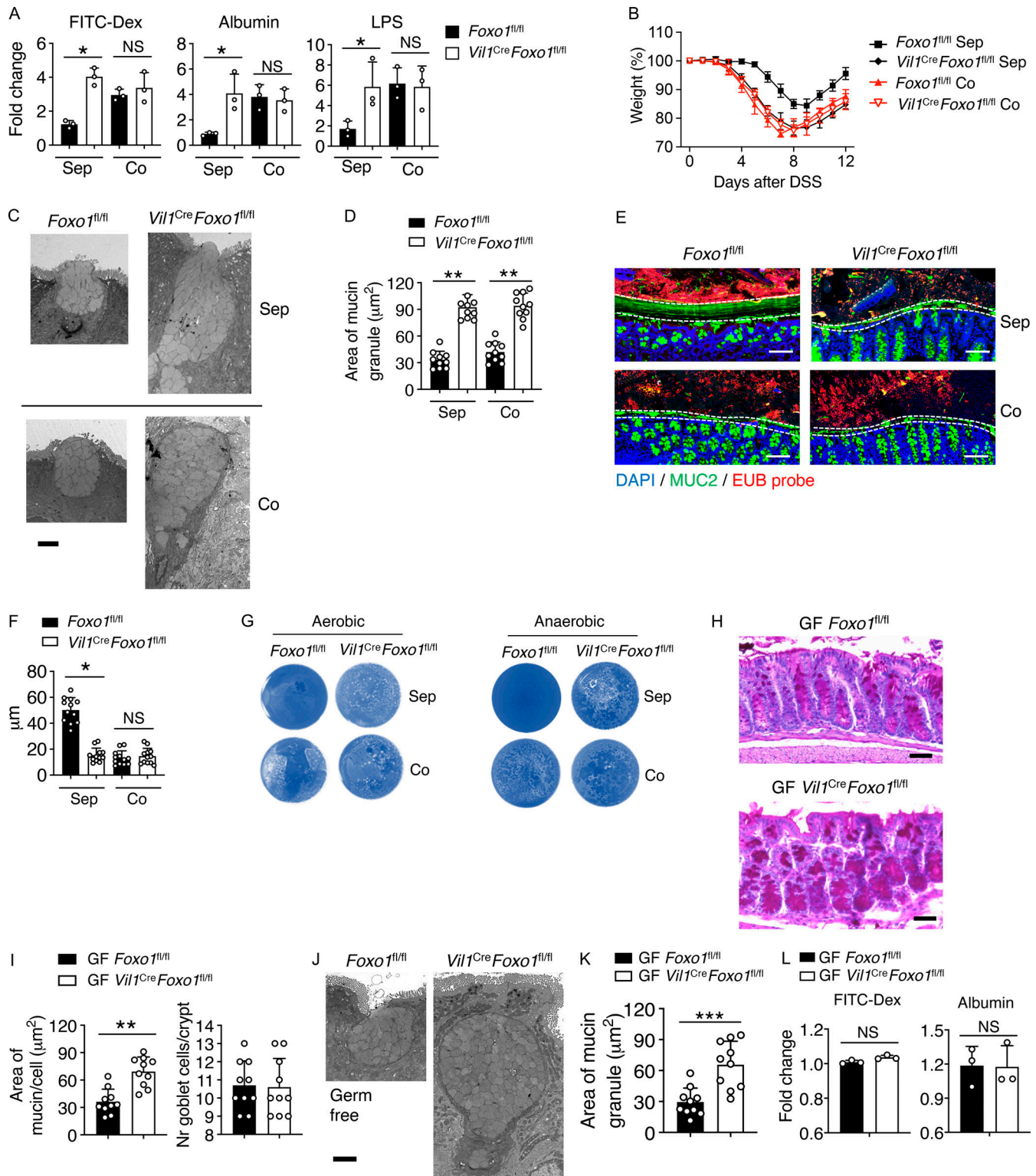


Figure 4. **IEC-derived Foxo1 regulates intestinal barrier integrity via gut microbiota.** (A) Intestinal barrier permeability was assessed by FITC-dextran (FITC-Dex), albumin, and LPS assays between *Foxo1<sup>fl/fl</sup>* and *Vil1<sup>Cre</sup>Foxo1<sup>fl/fl</sup>* mice under either separated (Sep) housing or cohousing (Co) conditions. (B) Body weights of *Foxo1<sup>fl/fl</sup>* and *Vil1<sup>Cre</sup>Foxo1<sup>fl/fl</sup>* mice under either separated housing or cohousing condition during DSS-induced colitis. (C) TEM images of upper crypt goblet cells from *Foxo1<sup>fl/fl</sup>* and *Vil1<sup>Cre</sup>Foxo1<sup>fl/fl</sup>* murine colons under either the separated housing or cohousing condition. Scale bar, 2 μm. (D) Quantification of average mucin granule area from C. (E) Representative immunofluorescence staining of colons from *Foxo1<sup>fl/fl</sup>* and *Vil1<sup>Cre</sup>Foxo1<sup>fl/fl</sup>* mice for mucus using MUC2 (green) and EUB338 probe (red) with DAPI (blue) under either separated housing or cohousing conditions. The white dashed lines outline the inner mucus layer. Scale bar, 50 μm. (F) Quantification of inner mucus layer thickness in the distal colon between *Foxo1<sup>fl/fl</sup>* and *Vil1<sup>Cre</sup>Foxo1<sup>fl/fl</sup>* mice under either separated housing or cohousing conditions (>10 fields measured per mouse). (G) Mucin lysis activity of fecal bacteria from *Foxo1<sup>fl/fl</sup>* and *Vil1<sup>Cre</sup>Foxo1<sup>fl/fl</sup>* mice under either separated housing or cohousing conditions was assessed by amido black staining under aerobic or anaerobic conditions. (H) PAS staining of colons from 8-wk-old GF

*Foxo1<sup>fl/fl</sup>* and *Vil1<sup>Cre</sup>Foxo1<sup>fl/fl</sup>* mice. Scale bar, 100  $\mu$ m. **(I)** Quantification of average mucin area/goblet cell (left) and quantification of the average number of goblet cells per crypt (right) from H. >100 crypts were measured per mouse. **(J)** TEM images of upper crypt goblet cells from GF *Foxo1<sup>fl/fl</sup>* and *Vil1<sup>Cre</sup>Foxo1<sup>fl/fl</sup>* mice. Scale bar, 2  $\mu$ m. **(K)** Quantification of average mucin granule area from J. **(L)** Intestinal barrier permeability was assessed by FITC-dextran and albumin assays between GF *Foxo1<sup>fl/fl</sup>* and *Vil1<sup>Cre</sup>Foxo1<sup>fl/fl</sup>* mice. Data are representative of three independent experiments (A, C, D, F, G, H, and J) or are pooled from two independent experiments (B, E, I, K, and L). \*,  $P < 0.05$ ; \*\*,  $P < 0.01$ ; \*\*\*,  $P < 0.001$  (Student's *t* test; error bars represent SD).

Broad population changes were found, ranging from the phylum to genus levels, in comparisons of fecal microbiota from separately housed *Foxo1<sup>fl/fl</sup>* and *Vil1<sup>Cre</sup>Foxo1<sup>fl/fl</sup>* mice (Fig. 6, D and E). Taxonomic classifications at the phylum level also suggested similar changes when we compared fecal microbiota from *Foxo1<sup>fl/fl</sup>* mice under separated housing and cohousing conditions (Fig. 6 F). Notably, the altered microbiome in *Foxo1*-deficient mice, such as increased Deferribacteres (Sun et al., 2019b), Proteobacteria (Gophna et al., 2006; Lo Presti et al., 2019; Lupp et al., 2007; Vester-Andersen et al., 2019), Actinobacteria (Alam et al., 2020; Lo Presti et al., 2019), and dampened Verrucomicrobia (Lo Presti et al., 2019; Salem et al., 2019), has been reported to be associated with either inflammatory bowel disease (IBD) patients or animal colitis models (Fig. 6 G). Additionally, detailed analysis revealed highly enriched mucin-degrading bacteria in the *Vil1<sup>Cre</sup>Foxo1<sup>fl/fl</sup>* and cohoused mice compared with separately housed *Foxo1<sup>fl/fl</sup>* control mice (Bell et al., 2019; Hoskins et al., 1997; Katayama et al., 2005; Wright et al., 2000; Fig. 6 H). This is consistent with the elevated mucinase activity in fecal bacteria found in *Vil1<sup>Cre</sup>Foxo1<sup>fl/fl</sup>* mice (Fig. S4 J and Fig. 5 G).

#### IEC-derived Foxo1 maintains epithelial TJs through bacterial SCFA metabolism

From the 16S rDNA-sequencing data, we further noticed that the abolished bacteria in *Vil1<sup>Cre</sup>Foxo1<sup>fl/fl</sup>* mice are known to be critical for production of SCFAs (Hugenholtz et al., 2018; Wang et al., 2019; Zhong et al., 2015; Fig. 7 A). In fact, our metabolomics study of SCFAs showed marked reduction of acetate, butyrate, and propionate in *Vil1<sup>Cre</sup>Foxo1<sup>fl/fl</sup>* compared with WT fecal samples (Fig. 7 B). It has previously been reported that loss of SCFAs in the intestines affects barrier function and enhances inflammation via disruption of TJs (Koh et al., 2016; Miyoshi et al., 2008; Ohata et al., 2005; Peng et al., 2009; Zheng et al., 2017). Changes in the expression levels of TJ proteins or delocalization of TJ proteins, such as occludin, also induce enhanced intestinal barrier permeability (Clayburgh et al., 2005; Lee et al., 2015). In fact, we observed disassociated occludin and F-actin at the colonic crypts of IECs in *Vil1<sup>Cre</sup>Foxo1<sup>fl/fl</sup>* mice, while these two proteins were clearly colocalized in *Foxo1<sup>fl/fl</sup>* mice (Fig. 7, C and D). *Foxo1<sup>fl/fl</sup>* mice exhibited a loss of colocalization of occludin and F-actin when cohoused with *Vil1<sup>Cre</sup>Foxo1<sup>fl/fl</sup>* mice (Fig. 7, C and D), consistent with compromised barrier permeability as compared with the separate housing condition (Fig. 4 A).

To further determine whether SCFAs were responsible for disrupted epithelial barrier function in *Vil1<sup>Cre</sup>Foxo1<sup>fl/fl</sup>* mice, we fed mice diets with supplementary acetate, propionate, butyrate, or succinate. We found that diet supplementation for 4 wk with the SCFAs acetate, propionate, and butyrate improved intestinal barrier function and reduced DSS-induced colitis severity in

*Vil1<sup>Cre</sup>Foxo1<sup>fl/fl</sup>* mice, whereas succinate did not (Fig. 7, E and F). Furthermore, occludin and F-actin association in colonic TJs was restored in *Vil1<sup>Cre</sup>Foxo1<sup>fl/fl</sup>* mice by dietary supplementation with acetate, propionate, and butyrate but not with succinate (Fig. S5, A and B). These results illustrate that the dysregulated microbiota observed in *Vil1<sup>Cre</sup>Foxo1<sup>fl/fl</sup>* affect production of metabolites, including SCFAs, that impair cellular localization of TJs, leading to disrupted barrier integrity and enhanced susceptibility to inflammation.

Lastly, to show a causal relationship between a specific species of microbiota and susceptibility to DSS-mediated colitis, we examined the alteration of a specific bacterium, *Akkermansia muciniphila*, between *Foxo1<sup>fl/fl</sup>* and *Vil1<sup>Cre</sup>Foxo1<sup>fl/fl</sup>* mice, given the abolished *Akkermansia* in *Foxo1*-deficient mice (Fig. 7 A). *A. muciniphila* has previously been demonstrated to protect the host from intestinal inflammation (Bian et al., 2019; Kang et al., 2013). We found that *A. muciniphila* was indeed diminished in the feces of separated *Vil1<sup>Cre</sup>Foxo1<sup>fl/fl</sup>* mice by quantitative PCR (qPCR; Fig. S5 C). We treated mice with *A. muciniphila* (BAA-835; American Type Culture Collection) for 2 wk by oral gavage as previously described (Bian et al., 2019), and we found enhanced acetate, butyrate, and propionate levels in the feces from *Vil1<sup>Cre</sup>Foxo1<sup>fl/fl</sup>* mice with *A. muciniphila* treatment compared with control mice (Fig. S5 D). Moreover, administration of *A. muciniphila* also improved intestinal barrier function and attenuated DSS-induced colitis in *Vil1<sup>Cre</sup>Foxo1<sup>fl/fl</sup>* mice (Fig. S5, E and F). These results indicate that decreased *A. muciniphila* contributes to enhanced susceptibility to colitis in *Vil1<sup>Cre</sup>Foxo1<sup>fl/fl</sup>* mice.

#### Discussion

The mutual interactions between IECs and gut microbiota form a dynamic ecosystem that maintains intestinal homeostasis. However, exactly how IECs regulate commensalism, leading to intestinal tolerance, is not yet fully elucidated. Our work demonstrates that cytosolic Foxo1 within goblet cells plays a critical role in promoting mucus layer formation by regulating mucin secretion in a process linked to autophagy. Formation and maintenance of mucus layer integrity is required for stabilization of the commensal microbiota and maintenance of intestinal barrier integrity. Loss of Foxo1 in IECs causes impaired mucus layer formation and subsequent dysbiosis, resulting in disrupted intestinal barrier integrity and enhanced susceptibility to infection and tissue inflammation.

Foxo1 function is regulated by post-transcriptional modifications, and phosphorylation of Foxo1 results in its nuclear export and relocation to the cytoplasm (Hedrick et al., 2012; Huang and Tindall, 2007). In our studies, nuclear retention of Foxo1 prevented normal mucus layer secretion from goblet cells. Activated Akt, which induces Foxo1 phosphorylation, is found in

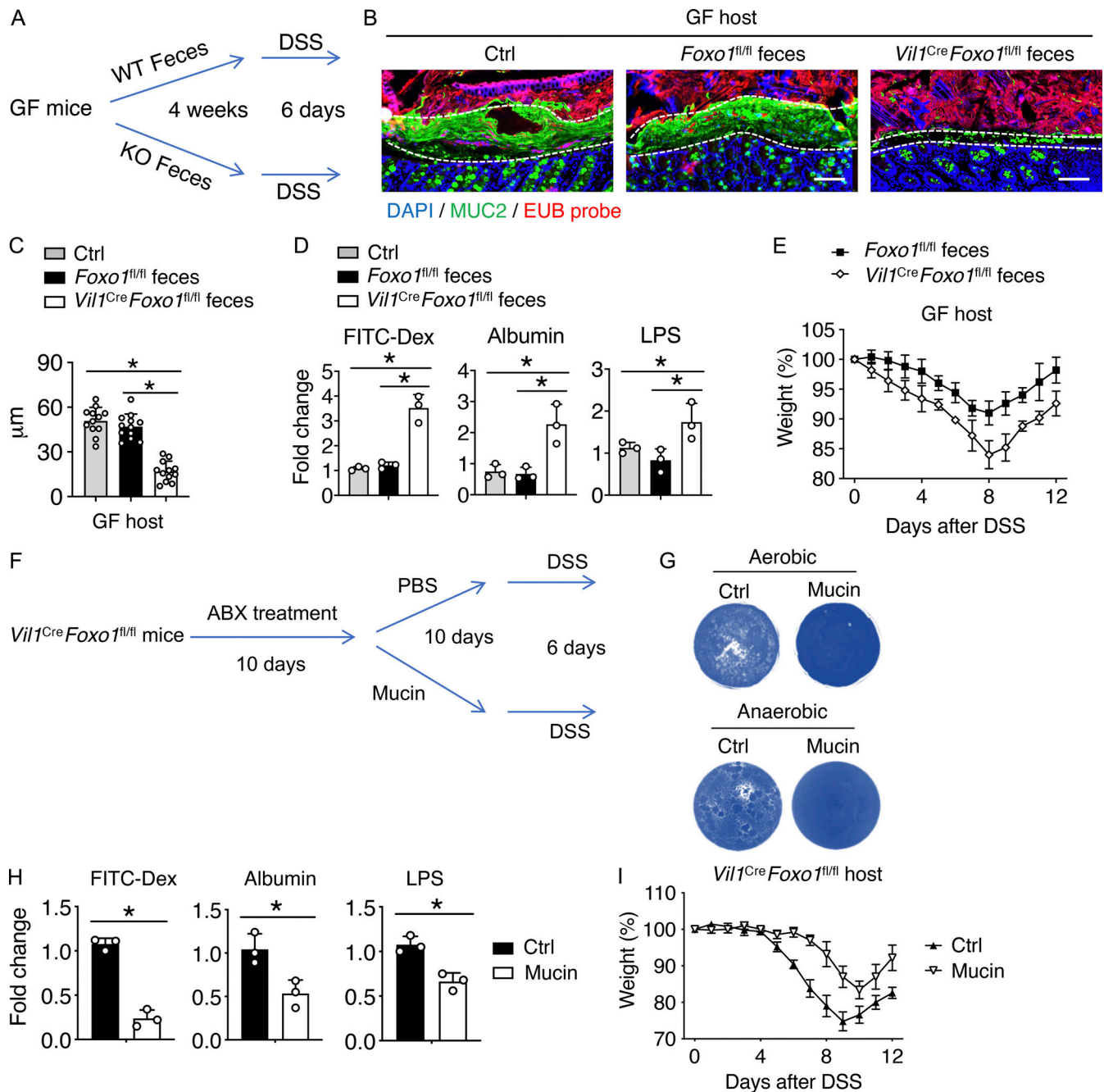
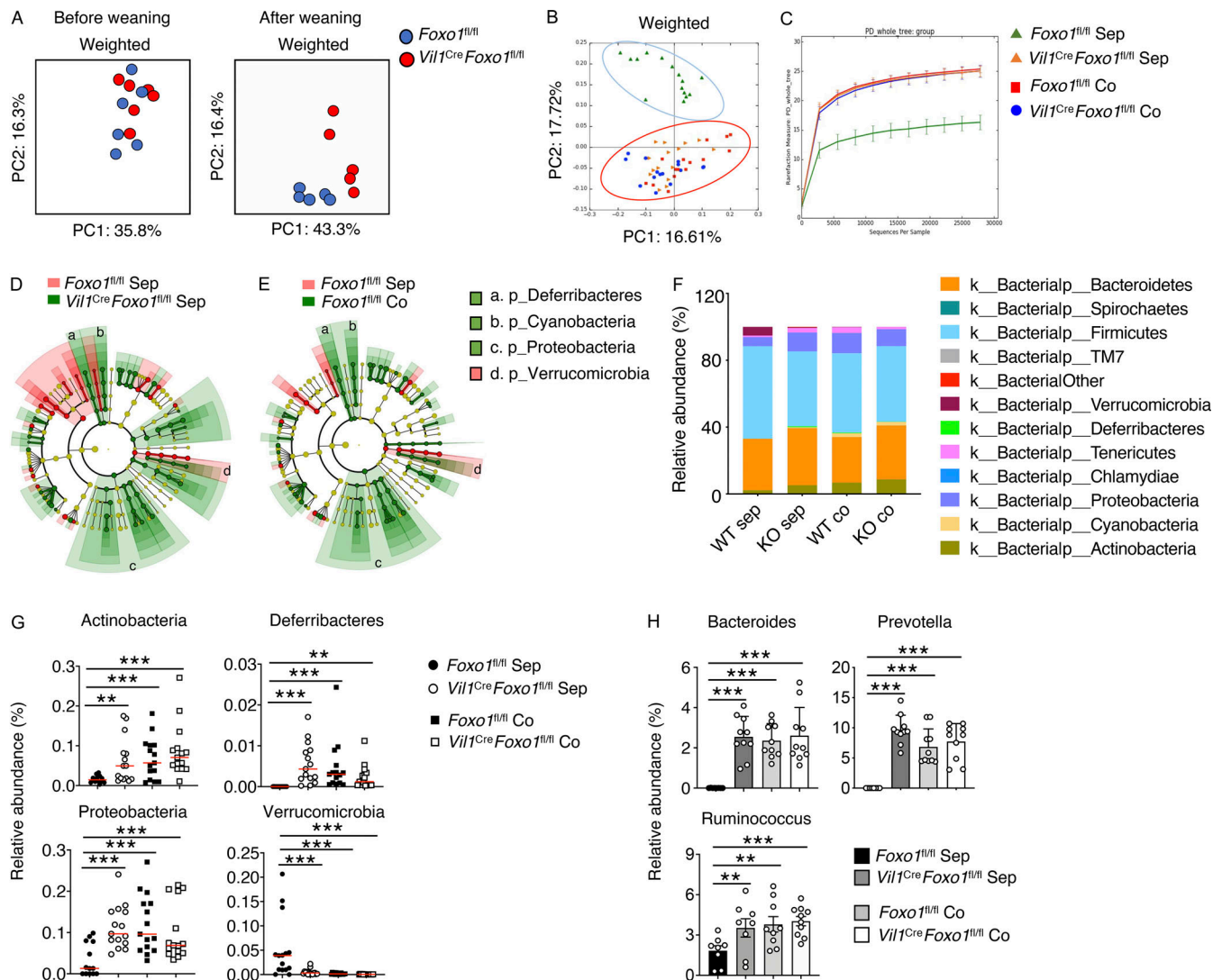


Figure 5. **IEC-derived Foxo1 governs bidirectional regulation of mucus and the gut microbiota.** (A) Schematic illustration of fecal transplant and DSS treatment from WT GF hosts. (B) Representative immunofluorescence staining in the colon of GF WT mice with fecal transplant for mucus using MUC2 (green) and EUB338 probe (red) with DAPI (blue). The white dashed lines outline the inner mucus layer. Scale bar, 50 μm. (C) Quantification of inner mucus layer thickness in the colon of GF *Foxo1<sup>fl/fl</sup>* mice with fecal transplant as in B (>10 fields measured per mouse). (D) Intestinal barrier permeability was assessed by FITC-dextran (FITC-Dex), albumin, and LPS assays of GF *Foxo1<sup>fl/fl</sup>* mice with fecal transplant. (E) Body weights of GF WT mice after *Foxo1<sup>fl/fl</sup>* or *Vil1<sup>Cre</sup>Foxo1<sup>fl/fl</sup>* fecal transplant during DSS-induced colitis. (F) Schematic illustration of mucin protein and DSS treatment in *Vil1<sup>Cre</sup>Foxo1<sup>fl/fl</sup>* mice. ABX, antibiotics. (G) Mucin lysis activity of fecal bacteria from *Foxo1<sup>fl/fl</sup>* and *Vil1<sup>Cre</sup>Foxo1<sup>fl/fl</sup>* mice under either separated housing or cohousing conditions was assessed by amide black staining under aerobic or anaerobic condition. (H) Intestinal barrier permeability was assessed by FITC-dextran, albumin, and LPS assays in *Vil1<sup>Cre</sup>Foxo1<sup>fl/fl</sup>* mice with indicated treatment. (I) Body weights of *Vil1<sup>Cre</sup>Foxo1<sup>fl/fl</sup>* mice with indicated treatment during DSS-induced colitis. Data are representative of two independent experiments (B, D, G, and H) or are pooled from two independent experiments (C, E, and I). \*, P < 0.05 (Student's *t* test; error bars represent SD).

constitutively high levels within goblet cells and extruding cells in the intestine, which can lead to restriction of Foxo1 to the cytoplasm (Gessain et al., 2015). The microbial danger signals detected by TLRs promote phosphorylation of Akt/PI3K (Kieser

and Kagan, 2017). Hence, gut commensal bacteria may contribute to maintenance of phosphorylation of Foxo1 within IECs, regulating goblet cell autophagy and mucus secretion. Consistent with our observations, constitutive activation of Foxo



**Figure 6. IEC-derived Foxo1 deficiency results in colonic dysbiosis.** (A) Principal coordinate (PC) analysis (PCoA) of weighted unique fraction metric (UniFrac) distances for 16S rDNA of the fecal bacteria composition from *Foxo1<sup>fl/fl</sup>* and *Vil1<sup>Cre</sup>Foxo1<sup>fl/fl</sup>* mice before weaning (3 wk old) and after weaning (6 wk old). (B) PCoA of weighted UniFrac distances for 16S rDNA of the fecal bacteria composition from *Foxo1<sup>fl/fl</sup>* and *Vil1<sup>Cre</sup>Foxo1<sup>fl/fl</sup>* mice under separated (Sep) housing or cohousing (Co) conditions. (C) Rarefaction curve constructed on the basis of phylogenetic distance (PD<sub>whole\_tree</sub>) from *Foxo1<sup>fl/fl</sup>* and *Vil1<sup>Cre</sup>Foxo1<sup>fl/fl</sup>* mice under either separated housing or cohousing conditions. (D) Cladogram representing taxa enriched in fecal samples in *Foxo1<sup>fl/fl</sup>* and *Vil1<sup>Cre</sup>Foxo1<sup>fl/fl</sup>* mice under separated housing condition. (E) Cladogram representing taxa enriched in fecal samples in *Foxo1<sup>fl/fl</sup>* mice under separated housing or cohousing conditions. (F) Taxonomic classifications at the phylum level for 16S rDNA of indicated bacteria in fecal samples from *Foxo1<sup>fl/fl</sup>* and *Vil1<sup>Cre</sup>Foxo1<sup>fl/fl</sup>* mice under separated housing or cohousing conditions. (G) Relative abundance of indicated bacterial phyla in fecal samples from different groups. (H) Relative abundance of indicated bacterial genera in fecal samples from different groups. Data are representative of two independent experiments (A–H). \*\*,  $P < 0.01$ ; \*\*\*,  $P < 0.001$  (Student's *t* test; error bars represent SD).

within IECs in *Drosophila* induces disruption of innate immune signals, leading to dysbiosis (Guo et al., 2014). Foxo1 is also critical for endothelial cell quiescence via restriction of cell metabolism. Forced expression of nuclear Foxo1 restricts endothelial cell proliferation and results in vessel thinning (Wilhelm et al., 2016). Additionally, continued nuclear Foxo1 expression within T cells induces Akt activation and disrupts mTORC1 signaling, inducing cell death (Newton et al., 2018). Therefore, although we observed impaired intestinal barrier integrity in both *Vil1<sup>Cre</sup>Foxo1<sup>fl/fl</sup>/Foxo1<sup>AAA/+</sup>* and *Vil1<sup>Cre</sup>Foxo1<sup>fl/fl</sup>* mice, it is possible that enforced nuclear Foxo1 expression in *Foxo1<sup>AAA</sup>* mice led to disruption of the intestinal barrier not only by affecting goblet

cell autophagy but also by interfering with IEC survival and division. Moreover, while it has been reported that Foxo family members have certain redundancies (Furuyama et al., 2000; Paik et al., 2007), our mRNA-seq data showed no up-regulated expression of other Foxo family members in the Foxo1-deficient IECs. Also, considering that both Foxo3- and Foxo4-deficient mice exhibit enhanced susceptibility to DSS-induced colitis (Snoeks et al., 2009; Zhou et al., 2009), there is unlikely to be a compensatory effect of Foxo3 or Foxo4 in the absence of Foxo1 for IEC homeostasis.

Autophagy as a biological process is critical for granule content secretion in primary IEC types, including goblet cells, Paneth cells, and osteoclasts (DeSelm et al., 2011; Patel et al.,

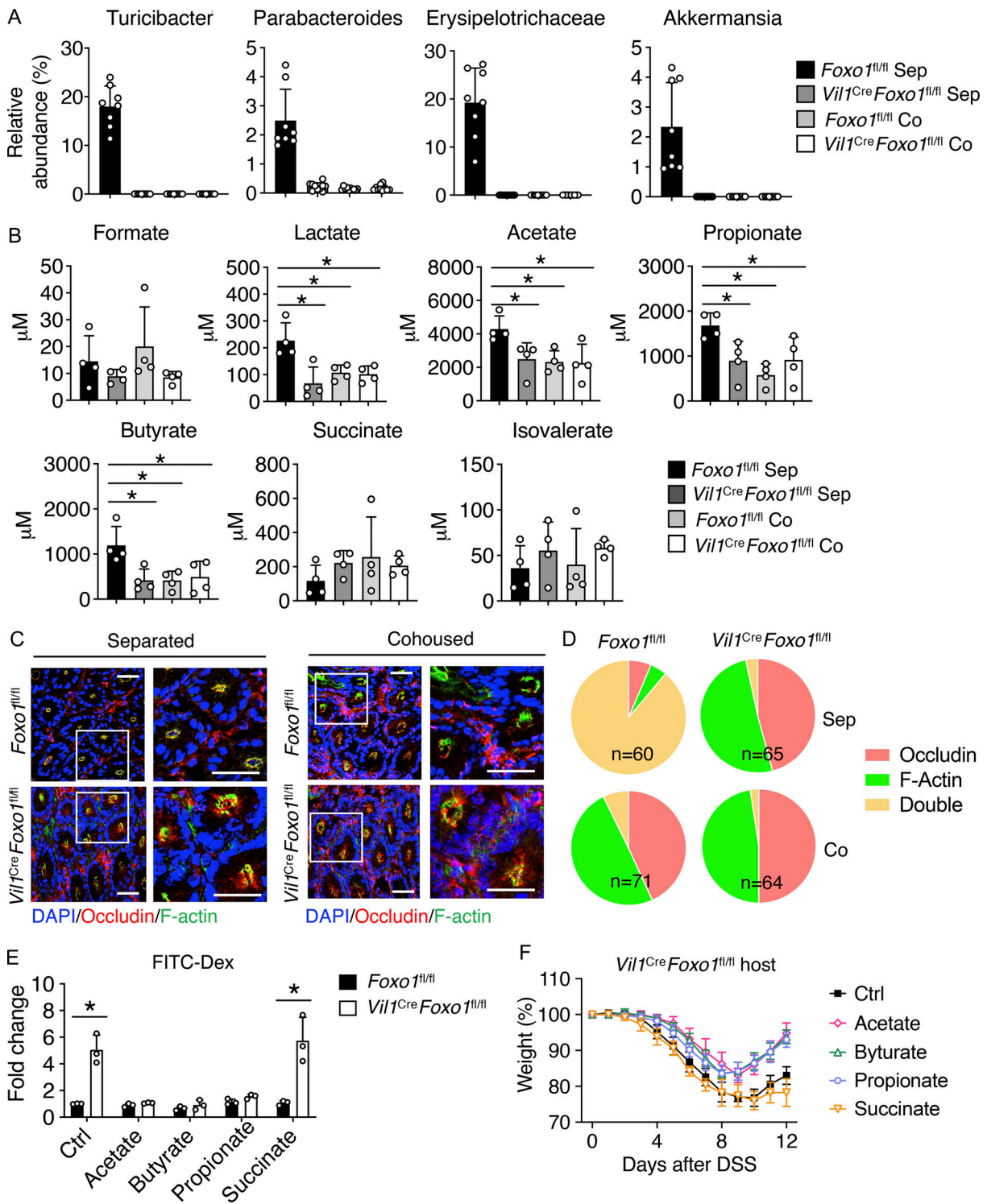


Figure 7. **IEC-derived Foxo1 maintains epithelial TJs through bacterial SCFA metabolism.** (A) Relative abundance of indicated bacterial genera in fecal samples from different groups. (B) Quantification of indicated SCFAs from feces of  $Foxo1^{fl/fl}$  and  $Vil1^{Cre}Foxo1^{fl/fl}$  mice under separated (Sep) housing and cohousing (Co) conditions. (C) Representative immunofluorescence staining for mucus using occludin (red) or F-actin (green) with DAPI (blue) distal colon segments between  $Foxo1^{fl/fl}$  and  $Vil1^{Cre}Foxo1^{fl/fl}$  mice under separated housing (left) or cohousing (right) condition. The right column represents a magnified image from the white box in the left column. Scale bar, 15  $\mu$ m. (D) Quantitative analysis of occludin colocalization with F-actin in colonic IECs as in G. Occludin, occluding-positive cells, no colocalization; F-actin, F-actin single-positive cells, no colocalization; Double, occludin and F-actin double-positive cells. (E) Intestinal barrier permeability was assessed by FITC-dextran (FITC-Dex) assay between  $Foxo1^{fl/fl}$  and  $Vil1^{Cre}Foxo1^{fl/fl}$  mice under the indicated treatment. (F) Body weights of  $Vil1^{Cre}Foxo1^{fl/fl}$  mice with the indicated treatment during DSS-induced colitis. Data are representative of two independent experiments (A, C, E, and F) or are pooled from two independent experiments (B and D). \*,  $P < 0.05$  (Student's  $t$  test; error bars represent SD).

2013; Wlodarska et al., 2014). The molecular mechanisms by which autophagy regulates the function of different cells are distinct (Cadwell et al., 2008; DeSelm et al., 2011; Mariño et al., 2010; Ushio et al., 2011). Foxo family members have been shown to regulate autophagy in multiple species, ranging from flies to mammals, and in different ways (Eijkelenboom and Burgering, 2013). Foxo3 and Foxo4 regulate the induction of autophagy by promoting glutamine synthetase (van der Vos and Coffey, 2012), while cytosolic Foxo1 interaction with ATG7 is critical for autophagy induction in tumor cells, resulting in cell death (Zhao et al., 2010). Our findings indicate that ATG5, an E2-like protein, interacts with Foxo1 in IECs. ATG5 has been reported to participate in autophagosome formation, which is required for epithelial secretory function by regulating ROS generation and calcium signaling (Patel et al., 2013). Although our results indicate that Foxo1 facilitates autophagy by interacting with ATG5 for mucin granule release, specifically how this interaction influences the autophagy process still requires further investigation. Meanwhile, autophagy has been linked to development of IBD in humans (Iida et al., 2017). Both human and mouse studies suggest that epithelial autophagy is required for intestinal homeostasis and host defense against pathogenic bacteria. Consistent with previous studies (Benjamin et al., 2013; Burger et al., 2018; Lavoie et al., 2019), we demonstrate here that compromised intestinal epithelial autophagy causes dysbiosis as well as disruption of immune regulation and barrier integrity.

The mucus layer is highly related to microbial colonization and motility (Caldara et al., 2012; Juge, 2012). Loss of mucus results in disrupted intestinal homeostasis and enhanced susceptibility to bacterial invasion (Shan et al., 2013). In addition, mucus has been shown to be critical for host defense by segregating and dissociating bacteria from the intestinal mucosa (McGuckin et al., 2011). In the colon, bacteria can use mucin glycans for anchor sites and as nutritional sources for growth (Marcobal et al., 2013; Pudlo et al., 2015). It has also been reported that the specific mucus component Lypd8 modulates flagellated bacteria motility and subsequently influences bacterial invasion into intestinal tissue (Okumura et al., 2016). Moreover, mucin glycosylation could be distinct in different mouse strains and living conditions. This could lead to selective bacterial colonization in different hosts (Ley et al., 2008; Rawls et al., 2006). Defects in the mucus layer are known to promote pathogenic bacterial invasion, such as *Citrobacter rodentium*, which invades the epithelium by producing virulence factors with mucinase activity (Bergstrom et al., 2010). We found that loss of Foxo1 impairs mucin secretion and inner mucus layer construction, which partially explains an increase in the abundance of bacteria with high mucinase activity. Additionally, it is known that AMPs are enriched in the mucus layer and are critical for tissue protection from bacterial invasion (Vaishnava et al., 2011). Although AMPs were expressed at similar levels in IECs from Foxo1<sup>fl/fl</sup> and Vili<sup>Cre</sup>Foxo1<sup>fl/fl</sup> mice, a failure to sequester AMPs in the disrupted mucus layer may contribute to dysbiosis in Vili<sup>Cre</sup>Foxo1<sup>fl/fl</sup> mice.

Similar to Foxo1-deficient mice, mucus defect-derived dysbiosis in *Muc2*<sup>-/-</sup> mice exhibits an enhanced bacterial diversity and elevated bacterial genera of *Ruminococcus* and *Bacteroides* (Wu et al., 2018b). Recent studies show that mice with disrupted mucus glycosylation display a compromised mucus barrier,

associated with decreased *A. muciniphila* and *Turicibacter* sp. H121 and with increases in the genus *Bacteroides* (Bergstrom et al., 2020), which is also in line with our findings of Foxo1 deficiency-induced dysbiosis. Additionally, we observed elevated Proteobacteria in the Foxo1-deficient mice, which usually can be found in mice with an increased inflammatory tone (Huang et al., 2015; Jakobsson et al., 2015). These studies support our conclusion that Foxo1-mediated mucus secretion is critical for commensalism and gut homeostasis. On the other hand, it has been reported that IBD patients exhibit thinner mucus layers due to impaired mucin production, secretion, or composition (Birchenough et al., 2019; Cornick et al., 2015; Etienne-Mesmin et al., 2019; Johansson and Hansson, 2016). However, there is a disproportionate amount of mucin-degrading bacteria in patients, which we also observed in Foxo1-deficient mice, including an increase in *Ruminococcus gnavus* and *Ruminococcus torques*, but a decrease in *A. muciniphila* (Liu et al., 2021; Salem et al., 2019), suggesting that the expansion of mucin-degrading bacteria does not depend entirely on the availability of mucus.

Bacteria-derived metabolites of SCFAs are known to regulate TJ permeability in different ways. For example, butyrate has been reported to enhance the expression of various TJ genes, including cingulin, zonula occludens 1 (ZO-1), ZO-2, claudin-1, claudin-3, and claudin-4, via regulation of histone acetylation (Waldecker et al., 2008). SCFAs are also known to be important for the assembly of TJs by enhancing adenosine monophosphate-activated protein kinase activity (Peng et al., 2009; Wang et al., 2012; Zhang et al., 2006). On the other hand, Foxo1 is found to restrict expression of ZO-1, claudin-3, and claudin-5 (Haines et al., 2016; Sun et al., 2019a; Taddei et al., 2008), which counteracts the effect of SCFAs on TJ expression. This could explain why we detected no differences in expression but found misplacement of occludin in Vili<sup>Cre</sup>Foxo1<sup>fl/fl</sup> mice. Furthermore, bacterial SCFAs are known to promote mucus production and secretion (Barcelo et al., 2000; Cornick et al., 2015; Willemsen et al., 2003). The loss of SCFA-producing bacteria may further dampen the mucus defect in Foxo1-deficient mice. Although it is known that SCFAs are critical for regulating intestinal immune responses (Arpaia et al., 2013; Mao et al., 2018; Olszak et al., 2014; Sun et al., 2018), we did not observe any defects in immune cell frequency in Vili<sup>Cre</sup>Foxo1<sup>fl/fl</sup> mice under the steady state (data not shown). Therefore, our data suggest that loss of Foxo1 induces a primary defect in mucus secretion by goblet cells and also has secondary effects, including dysbiosis, which may further amplify the dysregulation of intestinal barrier function.

In conclusion, we show in this study that IEC-derived cytosolic Foxo1 regulates mucus secretion, controlling gut commensalism and epithelial barrier integrity. Our data suggest that the host Foxo1 gene not only regulates goblet cell function but also influences gut bacterial composition, thereby identifying a novel host-microbiota positive feedback loop that is critical for maintaining intestinal homeostasis.

## Materials and methods

### Animals

C57BL/6 (WT), *Ngn3*<sup>Cre</sup>, *Math1*<sup>Cre</sup>, and Vili<sup>Cre</sup> mice were purchased from The Jackson Laboratory. *Defa6*<sup>Cre</sup> mice have been

described previously (Adolph et al., 2013). *Foxo1<sup>fl/fl</sup>* and *Foxo1<sup>AAA</sup>* mice were from Dr. Ming Li. All experiments were performed in accordance with guidelines prescribed by the institutional animal care and use committee at Harvard Medical School and the institutional animal care and use committee at the National Cancer Institute. All the experiments were restrictedly performed with littermate controls. *Vil1<sup>Cre</sup>Foxo1<sup>fl/+</sup>* and *Foxo1<sup>fl/fl</sup>* were used as breeders, and their offspring of *Vil1<sup>Cre</sup>Foxo1<sup>fl/fl</sup>* (*Foxo1<sup>ΔIEC</sup>*) and *Foxo1<sup>fl/fl</sup>* were used for our experiments. For cohousing experiments, 4-wk-old mice originating from the same breeders were divided to be either housed singly or co-housed with age- and sex-matched mice for 6 wk. The GF mice were generated in the GF animal facility in the Boston Children's Hospital.

### Intestinal barrier function assays

Mice were fasted overnight, and 3–5 kD FITC-dextran (Sigma-Aldrich) diluted in PBS was gavaged the following day. Fluorescence intensity in the serum was measured (excitation 485 nm/emission, 535 nm) 4 h after gavage. For fecal albumin assays, fecal pellets were weighed and homogenized. Albumin levels were quantified by ELISA according to the manufacturer's protocol (Bethyl Laboratories). LPS levels in mesenteric LN homogenates were assayed via the *Limulus* amoebocyte lysate test according to the manufacturer's protocol (Lonza). Albumin and LPS levels were normalized to fecal pellet or tissue weight and presented as fold differences relative to WT mice.

### IEC isolation

The mouse intestine tissues were isolated and opened longitudinally. After washing, the tissues were cut into small pieces and shaken in HBSS containing 5% FBS, 5 mM EDTA, and 1 mM dithiothreitol for 30 min. The remaining tissue was discarded, and epithelial cells in the supernatant were spun down at 150 *g* for 5 min.

### Mouse MUC2 isolation

Mucus was gently scraped off with a microscope slide from the mouse intestine, collected into 10-mm Petri dishes together with an equal volume of ice-cold PBS containing protease inhibitors, stirred gently at 4°C for 1 h, and centrifuged at 23,000 *g* for 45 min at 4°C. The extraction residue was incubated for 5 h at 37°C with 6 M guanidinium hydrochloride buffer supplemented with 10 mM of the reducing agent dithiothreitol. Overnight incubation with 25 mM iodoacetamide in the dark at room temperature was followed by centrifugation at 23,000 *g* for 45 min. The gel phase MUC2 was dialyzed with PBS at 4°C overnight using a Slide-A-Lyzer MINI dialysis cup. After removing LPS with the ToxinEraser Endotoxin Removal Kit, gel-forming mucins were concentrated with a SpeedVac apparatus and resuspended in PBS.

### Immunofluorescence and confocal microscopy

The isolated epithelial cells were fixed, blocked with 5% goat serum, and then incubated with anti-Foxo1 (Cell Signaling Technology) or anti-Muc2 (Santa Cruz Biotechnology). Slides were washed, incubated in Alexa Fluor 488- or Alexa Fluor 568-conjugated secondary antibodies (Invitrogen) containing DAPI and examined on an LSM 710 Zeiss confocal microscope.

### Intestinal organoid generation

The mice aged 6–10 wk were used to generate intestinal organoids as previously reported (Sato et al., 2009). Briefly, the small intestine was isolated and washed with cold PBS, and crypts were isolated following dissociation in EDTA. Isolated crypts were suspended in Matrigel. Following polymerization, IntestiCult Organoid Growth Medium (STEMCELL Technologies) was added and refreshed every 3–4 d. Organoids were maintained at 37°C and 5% CO<sub>2</sub> and propagated weekly.

For the induction of goblet cell-enriched differentiation, organoids were cultured in standard culture conditions and plated in Matrigel for 2 d. The organoids were then differentiated with the addition of IWP2 (N-[6-methyl-2-benzothiazolyl]-2-[(3,4,6,7-tetrahydro-4-oxo-3-phenylthieno[3,2-d]pyrimidin-2-yl)thio]-acetamide; 1.5 mM; Sigma-Aldrich) and DAPT (N-[N-(3,5-difluorophenacetyl)-L-alanyl]-S-phenylglycine *t*-butyl ester; 10 mM; Sigma-Aldrich) for 7 d. The organoid cells were released from Matrigel and fixed for immunofluorescence staining.

### Western blotting

The cells were lysed in radioimmunoprecipitation assay buffer (50 mM Tris-HCl, pH 7.5, 150 mM NaCl, 0.5% sodium deoxycholate, 0.2 mM EDTA, 10 mM Na<sub>3</sub>VO<sub>4</sub>, 10% glycerol, protease inhibitors) and centrifuged at 15,000 *g* for 15 min at 4°C. Then SDS loading buffer was added to the samples, and the samples were boiled for 10 min before the SDS-PAGE electrophoresis. Proteins were separated by PAGE using 4–12% NuPAGE Bis-Tris gels (Thermo Fisher Scientific) followed by transfer to nitrocellulose membranes. Membranes were incubated with 5% milk in TBST (0.5 M NaCl, Tris-HCl, pH 7.5, 0.1% [vol/vol] Tween-20) for 60 min and washed once with TBST. Proteins of interest were detected by incubating membranes overnight at 4°C in 5% BSA/TBST with anti-Foxo1 (Cell Signaling Technology), anti-REG3γ (Abgent), anti-lysozyme (Abcam), anti-ATG5 (Santa Cruz Biotechnology), anti-ATG7 (Abcam), anti-LC3 (Novus Biologicals), anti-β-tubulin (Thermo Fisher Scientific), anti-lamin B (Santa Cruz Biotechnology), anti-histone 3 (Cell Signaling Technology), or anti-β-actin (Sigma-Aldrich), washing with TBST three times for 10 min, and incubating with HRP-conjugated anti-rabbit or anti-mouse antibody (Cell Signaling Technology). Bound antibody was detected using Immobilon Western Chemiluminescent HRP Substrate (Thermo Fisher Scientific).

### Immunoprecipitation

Cell lysates were prepared as described above, and proteins were immunoprecipitated by incubation of lysates with 1 μg anti-Foxo1 antibody (Cell Signaling Technology) overnight at 4°C and pull-down of antibody-protein precipitates with Protein A/G Dynabeads (Invitrogen). Beads were washed extensively, and proteins were eluted with NuPAGE LDS sample buffer (10% 2-ME). The presence of immunocomplexed proteins was determined by Western blot analysis with the indicated antibodies.

### Quantitative RT-PCR

For gene expression detection, total RNA was isolated from whole cells using the Qiagen Mini RNA extraction kit following the manufacturer's instructions. RNA was quantified, and cDNA

was reverse transcribed using the iScript kit (Bio-Rad Laboratories) following the manufacturer's instructions. The cDNA samples were used at 20 ng/well in a 384-well plate and run in triplicate. PCRs were set up using TaqMan Universal PCR Master Mix (Applied Biosystems) on an ABI Prism 7500 Sequence Detection System. Quantification of relative mRNA expression was normalized to the expression of  $\beta$ -actin.

### ROS production measurement

The isolated epithelial cells were incubated with DCFDA dye (2',7'-dichlorofluorescein diacetate) from the Cellular ROS Assay Kit (Abcam) following the manufacturer's instructions. The quantification of ROS was detected by flow cytometry and with a fluorescent plate reader.

### Murine colitis model

Experimental colitis was initiated by treatment of mice with 2.5% DSS (36,000–50,000 mol wt; MP Biomedicals) in drinking water for 6 d. DSS was then replaced with normal water for another 6–7 d. Body weight was monitored daily. For mucin gavage, the mice were treated with an antibiotic cocktail (1 g/liter ampicillin, 1 g/liter neomycin, 1 g/liter metronidazole, 0.5 g/liter vancomycin) in drinking water for 3 wk. Then the mice were given normal water and gavaged with 200  $\mu$ l concentrated mucin at 1 mg/ml in PBS every other day for 10 d, and then DSS treatment was initiated. For fecal transplant, the GF mice were colonized via oral gavage twice with a stool suspension from the strains in the specific-pathogen-free condition, and after 4 wk, the DSS-induced colitis model was tested. For SCFA supplementation, 200 mM sodium acetate, 200 mM sodium propionate, or 200 mM sodium butyrate (Sigma-Aldrich) was administered in the drinking water for 3 wk before the DSS treatment.

### A. muciniphila culture and administration

*A. muciniphila* (BAA-835; American Type Culture Collection) was cultured in brain heart infusion medium (Gibco) plus 0.5% bovine submaxillary mucin at 37°C for 48 h under an anaerobic environment. *Vil1<sup>Cre</sup>Foxo1<sup>fl/fl</sup>* mice were administered 0.2 ml *A. muciniphila* ( $\sim 10^9$  CFU) once daily by oral gavage for 14 d. For the colitis model, the mice were given DSS in the drinking water after the first 7-d administration.

### Histology

Mouse intestine tissues were fixed in 10% formalin and preserved in 70% ethanol. Samples were then embedded in paraffin and cut into 10- $\mu$ m longitudinal sections, and H&E, PAS, and terminal deoxynucleotidyl transferase dUTP nick end labeling staining were performed by Histoserv Inc.

Pathology was scored from 0 to 5 in a blinded fashion. A score of 0 indicated no changes observed. A score of 1 indicated minimal scattered mucosal inflammatory cell infiltrates, with or without minimal epithelial hyperplasia. A score of 2 indicated mild scattered to diffuse inflammatory cell infiltrates, sometimes extending into the submucosa and associated with erosions, with minimal to mild epithelial hyperplasia and minimal to mild mucin depletion from goblet cells. A score of 3 indicated

mild to moderate inflammatory cell infiltrates that were sometimes transmural, often associated with ulceration, with moderate epithelial hyperplasia and mucin depletion. A score of 4 indicated marked inflammatory cell infiltrates that were often transmural and associated with ulceration, with marked epithelial hyperplasia and mucin depletion. A score of 5 indicated marked transmural inflammation with severe ulceration and loss of intestinal glands.

For immunofluorescence staining, slides were deparaffinized by xylene, and antigen retrieval was conducted for 20 min in a 95°C water bath in 10 mM sodium citrate, pH 6.0, followed by a 15-min incubation at room temperature. Slides were washed, blocked in 5% BSA, and stained with the primary antibodies anti-Ki67 (eBioscience), anti-lysozyme (Abcam), and anti-REG3 $\gamma$  (Abgent) and secondary antibodies conjugated to Alexa Fluor 488, 633, or 594 (Thermo Fisher Scientific). Slides were mounted in Fluoromount-G medium (Thermo Fisher Scientific), and 3–15 images were taken per slide at 20 $\times$  or 40 $\times$  magnification along transections of the intestinal crypts for each biological replicate (Zeiss).

For bacterial 16S rDNA FISH, the colon tissues were fixed in Carnoy's buffer (60% methanol, 30% chloroform, 10% acetic acid). The paraffin sections were incubated with EUB338 probe conjugated with Alexa Fluor 555 at 50°C followed by anti-MUC2 (Santa Cruz Biotechnology) staining.

For TJ protein staining, tissues were embedded in Tissue-Tek O.C.T. compound (Sakura Finetek) in cryomolds and snap frozen in liquid nitrogen for cryosectioning. Cryosections were prepared on a Leica Cryostat (Leica Microsystems) at  $-21^{\circ}\text{C}$  and 5- $\mu$ m thickness. Sections were mounted on glass slides and fixed in 100% ethanol at 4°C for 30 min followed by 3 min of  $-20^{\circ}\text{C}$  acetone fixation at room temperature. The tissue sections were stained with a monoclonal occludin antibody (OC-3F10; Life Technologies) and Alexa Fluor 546 phalloidin (Life Technologies).

### Whole-mount intestinal immunofluorescence

The experiment was performed according to the protocol on a continuously updated website (<https://idisco.info/>). Briefly, the colon tissues were cut longitudinally and fixed with 4% paraformaldehyde. After washing and methanol dehydration steps, whole-mount samples were permeabilized first in 0.2% Triton X-100 followed by 0.2% Triton X-100/20% DMSO/0.3 M glycine. The samples were blocked for 1–2 d in 1 $\times$  Dulbecco's PBS with 0.2% Triton X-100/10% DMSO/6% donkey serum at 37°C with gentle agitation. Fluorescein-conjugated UEA was added to the blocking buffer at appropriate concentrations and incubated 1–2 d at 37°C. Samples were then washed in 1 $\times$  Dulbecco's PBS with 0.2% Tween-20 and heparin (100 mg/ml), mounted in agarose, and cleared using dichloromethane followed by benzyl ether. Images were obtained using a confocal microscope (Zeiss) and analyzed using Imaris software.

### Transmission EM

Mouse distal colon tissues were fixed with 2.5% glutaraldehyde and 2.0% paraformaldehyde in 0.1 M sodium cacodylate buffer, pH 7.4. The samples were processed in the Harvard Medical

School Electron Microscopy Facility. The sections were observed with a JEOL 1200EX 80-kV electron microscope.

### Mucinase activity assay

Fecal bacteria from WT and *Foxo1<sup>ΔIEC</sup>* mice under either the separated housing or cohousing condition were grown on *Bruccella* plates containing 0.5% bovine submaxillary mucin for 48 h under aerobic or anaerobic condition, and the plates were stained with 0.1% (wt/vol) amido black in 3.5 M acetic acid for 30 min and destained with 1.2 M acetic acid.

### RNA-seq

Total RNA was used for preparing RNA-seq libraries with the Illumina TruSeq RNA Sample Preparation Kit. Libraries were sequenced with single-end 75-bp reads on an Illumina NextSeq system. All analyses were performed in Partek Flow software version 5.0 (Partek Inc.). Fastq files were uploaded into Partek Flow software for processing, aligned using the STAR aligner, and quantified to the transcriptome (Partek E/M using mm10 Ensembl Transcripts release 94 as the reference index). The raw counts were further analyzed using the R package DESeq2. Adjusted P values <0.05 were deemed significant.

### 16S rRNA quantification and sequencing

Fecal samples were collected from live mice, snap frozen, and stored at  $-80^{\circ}\text{C}$ . DNA was extracted using the QIAamp DNA Stool Mini Kit (Qiagen). 0.1  $\mu\text{g}$  DNA was used for relative quantification by qPCR with the following primers: forward: 5'-GACCGCATGTTCAAGCAGACT-3' and reverse: 5'-AAGCCG CATTGGGATTATTTGTT-3' PCR for *A. muciniphila*; forward: 5'-TCCTACGGGAGGCAGCAGT-3' and reverse: 5'-GGACTACCA GGGTATCTATCCTGTT-3' for total bacteria. The PCRs were set up using SYBR PCR Master Mix (Applied Biosystems) on an ABI Prism 7500 Sequence Detection System. For sequencing, DNA samples were amplified using barcoded V4 region primers targeting the bacterial 16S rRNA gene and sequenced using an Illumina MiSeq sequencer. Sequence analysis was performed using the QIIME pipeline (Caporaso et al., 2010) with default settings. Linear discriminant analysis effect size (Segata et al., 2011) was used via the Galaxy Browser (Blankenberg et al., 2010) to detect significant changes in relative abundance of microbial taxa.

### SCFA measurement

The fecal samples were sent to the Protein Characterization Core at the National Cancer Institute. The SCFA concentrations were quantified by liquid chromatography/mass spectrometry according to a previous report (Han et al., 2015).

### Statistical analysis

Statistical analyses were performed with GraphPad Prism 5.0 software (GraphPad Software) using an unpaired two-tailed Student's *t* test. Statistical significance was defined as  $P < 0.05$ .

### Online supplemental material

Fig. S1 shows that *Foxo1* does not affect IEC proliferation and apoptosis. Fig. S2 shows that *Foxo1* deficiency in goblet cells

impairs intestinal barrier integrity. Fig. S3 shows that cytosolic *Foxo1* regulates goblet cell autophagy. Fig. S4 shows that IEC-derived *Foxo1* governs bidirectional regulation of mucus and gut microbiota. Fig. S5 shows that IEC-derived *Foxo1* maintains epithelial TJs through bacterial SCFA metabolism.

### Data availability

RNA-seq data from this study are publicly available from the National Center for Biotechnology Information Gene Expression Omnibus database (accession no. GSE178650).

## Acknowledgments

We thank Dr. Ming Li (Sloan Kettering Institute, New York, NY) for generously providing the *Foxo1<sup>ΔIEC</sup>* and *Foxo1<sup>AAA</sup>* mice. We thank Dr. Mary Collins for her advice and editing of the manuscript.

Z. Chen was supported by a fellowship from the Crohn's and Colitis Foundation (479689). S. Wang was supported by the American Diabetes Association (1-16-INI-16), the National Eye Institute (P30-EY026877), and an unrestricted grant from Research to Prevent Blindness. C. Wu was supported by a National Multiple Sclerosis Society Career Transition Award (TA 3059-A-2). V.K. Kuchroo was supported by the National Institutes of Health (R01 AI139536).

Author contributions: Z. Chen performed experiments and wrote the manuscript. J. Luo, J. Li, G. Kim, E.S. Chen, S. Xiao, and B. Bao performed experiments. S.B. Snapper, R.S. Blumberg, C. Lin, S. Wang, and D. An provided key materials. J. Zhong, K. Liu, and Q. Li analyzed the data. V.K. Kuchroo edited the manuscript. C. Wu designed, performed, and supervised the study and wrote the manuscript.

Disclosures: S.B. Snapper reported personal fees from Pandion, IFM Therapeutics, Hoffman La Roche, Amgen, Lilly, Takeda, Kyverna, Pfizer, Merck, and Third Rock outside the submitted work. S. Xiao is an employee of Celsius Therapeutics. V.K. Kuchroo has an ownership interest in and is a member of the scientific advisory board for Tizona Therapeutics, Bicara Therapeutics, Compass Therapeutics, Larkspur Biosciences, and Trishula Therapeutics. The interests of V.K. Kuchroo were reviewed and managed by the Brigham and Women's Hospital and Partners Healthcare in accordance with their conflict-of-interest policies. No other disclosures were reported.

Submitted: 8 February 2021

Revised: 18 May 2021

Accepted: 30 June 2021

## References

- Adolph, T.E., M.F. Tomczak, L. Niederreiter, H.J. Ko, J. Böck, E. Martinez-Naves, J.N. Glickman, M. Tschurtschenthaler, J. Hartwig, S. Hosomi, et al. 2013. Paneth cells as a site of origin for intestinal inflammation. *Nature*. 503:272-276. <https://doi.org/10.1038/nature12599>
- Alam, M.T., G.C.A. Amos, A.R.J. Murphy, S. Murch, E.M.H. Wellington, and R.P. Arasaradnam. 2020. Microbial imbalance in inflammatory bowel disease patients at different taxonomic levels. *Gut Pathog.* 12:1. <https://doi.org/10.1186/s13099-019-0341-6>

- Arpaia, N., C. Campbell, X. Fan, S. Dikiy, J. van der Veeke, P. deRoos, H. Liu, J.R. Cross, K. Pfeffer, P.J. Coffey, and A.Y. Rudensky. 2013. Metabolites produced by commensal bacteria promote peripheral regulatory T-cell generation. *Nature*. 504:451–455. <https://doi.org/10.1038/nature12726>
- Artis, D., and R.K. Grenics. 2008. The intestinal epithelium: sensors to effectors in nematode infection. *Mucosal Immunol.* 1:252–264. <https://doi.org/10.1038/mi.2008.21>
- Barcelo, A., J. Claustre, F. Moro, J.A. Chayvialle, J.C. Cuber, and P. Plaisancié. 2000. Mucin secretion is modulated by luminal factors in the isolated vascularly perfused rat colon. *Gut*. 46:218–224. <https://doi.org/10.1136/gut.46.2.218>
- Bel, S., M. Pendse, Y. Wang, Y. Li, K.A. Ruhn, B. Hassell, T. Leal, S.E. Winter, R.J. Xavier, and L.V. Hooper. 2017. Paneth cells secrete lysozyme via secretory autophagy during bacterial infection of the intestine. *Science*. 357:1047–1052. <https://doi.org/10.1126/science.aal4677>
- Belkaid, Y., and S. Tamoutounour. 2016. The influence of skin microorganisms on cutaneous immunity. *Nat. Rev. Immunol.* 16:353–366. <https://doi.org/10.1038/nri.2016.48>
- Bell, A., J. Brunt, E. Crost, L. Vaux, R. Nepravishta, C.D. Owen, D. Latousakis, A. Xiao, W. Li, X. Chen, et al. 2019. Elucidation of a sialic acid metabolism pathway in mucus-foraging *Ruminococcus gnavus* unravels mechanisms of bacterial adaptation to the gut. *Nat. Microbiol.* 4: 2393–2404. <https://doi.org/10.1038/s41564-019-0590-7>
- Benjamin, J.L., R. Sumpter Jr., B. Levine, and L.V. Hooper. 2013. Intestinal epithelial autophagy is essential for host defense against invasive bacteria. *Cell Host Microbe*. 13:723–734. <https://doi.org/10.1016/j.chom.2013.05.004>
- Bergstrom, K.S., V. Kissonog-Singh, D.L. Gibson, C. Ma, M. Montero, H.P. Sham, N. Ryz, T. Huang, A. Vclich, B.B. Finlay, et al. 2010. Muc2 protects against lethal infectious colitis by disassociating pathogenic and commensal bacteria from the colonic mucosa. *PLoS Pathog.* 6: e1000902. <https://doi.org/10.1371/journal.ppat.1000902>
- Bergstrom, K., X. Shan, D. Casero, A. Batushansky, V. Lagishetty, J.P. Jacobs, C. Hoover, Y. Kondo, B. Shao, L. Gao, et al. 2020. Proximal colon-derived O-glycosylated mucus encapsulates and modulates the microbiota. *Science*. 370:467–472. <https://doi.org/10.1126/science.aay7367>
- Bian, X., W. Wu, L. Yang, L. Lv, Q. Wang, Y. Li, J. Ye, D. Fang, J. Wu, X. Jiang, et al. 2019. Administration of *Akkermansia muciniphila* ameliorates dextran sulfate sodium-induced ulcerative colitis in mice. *Front. Microbiol.* 10:2259. <https://doi.org/10.3389/fmicb.2019.02259>
- Birchenough, G., B.O. Schroeder, F. Bäckhed, and G.C. Hansson. 2019. Dietary destabilisation of the balance between the microbiota and the colonic mucus barrier. *Gut Microbes*. 10:246–250. <https://doi.org/10.1080/19490976.2018.1513765>
- Blankenberg, D., G. Von Kuster, N. Coraor, G. Ananda, R. Lazarus, M. Mangana, A. Nekrutenko, and J. Taylor. 2010. Galaxy: a web-based genome analysis tool for experimentalists. *Curr. Protoc. Mol. Biol.* Chapter 19: 10.1–21. <https://doi.org/10.1002/0471142727.mb1910s89>
- Buffie, C.G., and E.G. Pamer. 2013. Microbiota-mediated colonization resistance against intestinal pathogens. *Nat. Rev. Immunol.* 13:790–801. <https://doi.org/10.1038/nri3535>
- Burger, E., A. Araujo, A. López-Yglesias, M.W. Rajala, L. Geng, B. Levine, L.V. Hooper, E. Burstein, and F. Yarovinsky. 2018. Loss of Paneth cell autophagy causes acute susceptibility to *Toxoplasma gondii*-mediated inflammation. *Cell Host Microbe*. 23:177–190.e4. <https://doi.org/10.1016/j.chom.2018.01.001>
- Cadwell, K., J.Y. Liu, S.L. Brown, H. Miyoshi, J. Loh, J.K. Lennerz, C. Kishi, W. Kc, J.A. Carrero, S. Hunt, et al. 2008. A key role for autophagy and the autophagy gene *Atg16l1* in mouse and human intestinal Paneth cells. *Nature*. 456:259–263. <https://doi.org/10.1038/nature07416>
- Caldara, M., R.S. Friedlander, N.L. Kavanaugh, J. Aizenberg, K.R. Foster, and K. Ribbeck. 2012. Mucin biopolymers prevent bacterial aggregation by retaining cells in the free-swimming state. *Curr. Biol.* 22:2325–2330. <https://doi.org/10.1016/j.cub.2012.10.028>
- Caporaso, J.G., J. Kuczynski, J. Stombaugh, K. Bittinger, F.D. Bushman, E.K. Costello, N. Fierer, A.G. Peña, J.K. Goodrich, J.I. Gordon, et al. 2010. QIIME allows analysis of high-throughput community sequencing data. *Nat. Methods*. 7:335–336. <https://doi.org/10.1038/nmeth.f.303>
- Clayburgh, D.R., T.A. Barrett, Y. Tang, J.B. Meddings, L.J. Van Eldik, D.M. Watterson, L.L. Clarke, R.J. Mrsny, and J.R. Turner. 2005. Epithelial myosin light chain kinase-dependent barrier dysfunction mediates T cell activation-induced diarrhea in vivo. *J. Clin. Invest.* 115:2702–2715. <https://doi.org/10.1172/JCI24970>
- Cornick, S., A. Tawiah, and K. Chadee. 2015. Roles and regulation of the mucus barrier in the gut. *Tissue Barriers*. 3:e982426. <https://doi.org/10.4161/21688370.2014.982426>
- Desai, M.S., A.M. Seekatz, N.M. Koropatkin, N. Kamada, C.A. Hickey, M. Wolter, N.A. Pudlo, S. Kitamoto, N. Terrapon, A. Muller, et al. 2016. A dietary fiber-deprived gut microbiota degrades the colonic mucus barrier and enhances pathogen susceptibility. *Cell*. 167:1339–1353.e21. <https://doi.org/10.1016/j.cell.2016.10.043>
- DeSelm, C.J., B.C. Miller, W. Zou, W.L. Beatty, E. van Meel, Y. Takahata, J. Klumperman, S.A. Tooze, S.L. Teitelbaum, and H.W. Virgin. 2011. Autophagy proteins regulate the secretory component of osteoclastic bone resorption. *Dev. Cell*. 21:966–974. <https://doi.org/10.1016/j.devcel.2011.08.016>
- Eijkelenboom, A., and B.M. Burgering. 2013. FOXOs: signalling integrators for homeostasis maintenance. *Nat. Rev. Mol. Cell Biol.* 14:83–97. <https://doi.org/10.1038/nrm3507>
- Elinav, E., T. Strowig, A.L. Kau, J. Henao-Mejia, C.A. Thaiss, C.J. Booth, D.R. Peaper, J. Bertin, S.C. Eisenbarth, J.I. Gordon, and R.A. Flavell. 2011. NLRP6 inflammasome regulates colonic microbial ecology and risk for colitis. *Cell*. 145:745–757. <https://doi.org/10.1016/j.cell.2011.04.022>
- Etienne-Mesmin, L., B. Chassaing, M. Desvaux, K. De Paepe, R. Gresse, T. Sauvatre, E. Forano, T.V. de Wiele, S. Schüller, N. Juge, and S. Blanquet-Diot. 2019. Experimental models to study intestinal microbes-mucus interactions in health and disease. *FEMS Microbiol. Rev.* 43: 457–489. <https://doi.org/10.1093/femsre/fuz013>
- Furuyama, T., T. Nakazawa, I. Nakano, and N. Mori. 2000. Identification of the differential distribution patterns of mRNAs and consensus binding sequences for mouse DAF-16 homologues. *Biochem. J.* 349:629–634. <https://doi.org/10.1042/bj3490629>
- Gessain, G., Y.H. Tsai, L. Travier, M. Bonazzi, S. Grayo, P. Cossart, C. Charlier, O. Disson, and M. Lecuit. 2015. PI3-kinase activation is critical for host barrier permissiveness to *Listeria monocytogenes*. *J. Exp. Med.* 212: 165–183. <https://doi.org/10.1084/jem.20141406>
- Gill, N., M. Wlodarska, and B.B. Finlay. 2011. Roadblocks in the gut: barriers to enteric infection. *Cell. Microbiol.* 13:660–669. <https://doi.org/10.1111/j.1462-5822.2011.01578.x>
- Gophna, U., K. Sommerfeld, S. Gophna, W.F. Doolittle, and S.J. Veldhuyzen van Zanten. 2006. Differences between tissue-associated intestinal microfloras of patients with Crohn's disease and ulcerative colitis. *J. Clin. Microbiol.* 44:4136–4141. <https://doi.org/10.1128/JCM.01004-06>
- Guo, L., J. Karpac, S.L. Tran, and H. Jasper. 2014. PGRP-SC2 promotes gut immune homeostasis to limit commensal dysbiosis and extend lifespan. *Cell*. 156:109–122. <https://doi.org/10.1016/j.cell.2013.12.018>
- Haines, R.J., R.S. Beard Jr., R.A. Eitner, L. Chen, and M.H. Wu. 2016. TNFα/IFNγ mediated intestinal epithelial barrier dysfunction is attenuated by microRNA-93 downregulation of PTK6 in mouse colonic epithelial cells. *PLoS One*. 11:e0154351. <https://doi.org/10.1371/journal.pone.0154351>
- Han, J., K. Lin, C. Sequeira, and C.H. Borchers. 2015. An isotope-labeled chemical derivatization method for the quantitation of short-chain fatty acids in human feces by liquid chromatography-tandem mass spectrometry. *Anal. Chim. Acta.* 854:86–94. <https://doi.org/10.1016/j.aca.2014.11.015>
- Hedrick, S.M., R. Hess Michelini, A.L. Doedens, A.W. Goldrath, and E.L. Stone. 2012. FOXO transcription factors throughout T cell biology. *Nat. Rev. Immunol.* 12:649–661. <https://doi.org/10.1038/nri3278>
- Hoskins, L.C., E.T. Boulding, and G. Larson. 1997. Purification and characterization of blood group A-degrading isoforms of α-N-acetylgalactosaminidase from *Ruminococcus torques* strain IX-70. *J. Biol. Chem.* 272: 7932–7939. <https://doi.org/10.1074/jbc.272.12.7932>
- Huang, H., and D.J. Tindall. 2007. Dynamic FoxO transcription factors. *J. Cell Sci.* 120:2479–2487. <https://doi.org/10.1242/jcs.001222>
- Huang, E.Y., T. Inoue, V.A. Leone, S. Dalal, K. Touw, Y. Wang, M.W. Musch, B. Theriault, K. Higuchi, S. Donovan, et al. 2015. Using corticosteroids to reshape the gut microbiome: implications for inflammatory bowel diseases. *Inflamm. Bowel Dis.* 21:963–972. <https://doi.org/10.1097/MIB.0000000000000332>
- Hugenholtz, F., M. Davids, J. Schwarz, M. Müller, D. Tomé, P. Schaap, G.J.E.J. Hooiveld, H. Smid, and M. Kleerebezem. 2018. Metatranscriptome analysis of the microbial fermentation of dietary milk proteins in the murine gut. *PLoS One*. 13:e0194066. <https://doi.org/10.1371/journal.pone.0194066>
- Iida, T., K. Onodera, and H. Nakase. 2017. Role of autophagy in the pathogenesis of inflammatory bowel disease. *World J. Gastroenterol.* 23: 1944–1953. <https://doi.org/10.3748/wjg.v23.i11.1944>
- Jakobsson, H.E., A.M. Rodríguez-Piñero, A. Schütte, A. Ermund, P. Boysen, M. Bemark, F. Sommer, F. Bäckhed, G.C. Hansson, and M.E. Johansson. 2015. The composition of the gut microbiota shapes the colon mucus barrier. *EMBO Rep.* 16:164–177. <https://doi.org/10.15252/embr.201439263>

- Johansson, M.E., and G.C. Hansson. 2016. Immunological aspects of intestinal mucus and mucins. *Nat. Rev. Immunol.* 16:639–649. <https://doi.org/10.1038/nri.2016.88>
- Juge, N. 2012. Microbial adhesins to gastrointestinal mucus. *Trends Microbiol.* 20:30–39. <https://doi.org/10.1016/j.tim.2011.10.001>
- Kang, C.S., M. Ban, E.J. Choi, H.G. Moon, J.S. Jeon, D.K. Kim, S.K. Park, S.G. Jeon, T.Y. Roh, S.J. Myung, et al. 2013. Extracellular vesicles derived from gut microbiota, especially *Akkermansia muciniphila*, protect the progression of dextran sulfate sodium-induced colitis. *PLoS One.* 8: e76520. <https://doi.org/10.1371/journal.pone.0076520>
- Katayama, T., K. Fujita, and K. Yamamoto. 2005. Novel bifidobacterial glycosidases acting on sugar chains of mucin glycoproteins. *J. Biosci. Bioeng.* 99:457–465. <https://doi.org/10.1263/jbb.99.457>
- Kieser, K.J., and J.C. Kagan. 2017. Multi-receptor detection of individual bacterial products by the innate immune system. *Nat. Rev. Immunol.* 17: 376–390. <https://doi.org/10.1038/nri.2017.25>
- Koh, A., F. De Vadder, P. Kovatcheva-Datchary, and F. Bäckhed. 2016. From dietary fiber to host physiology: short-chain fatty acids as key bacterial metabolites. *Cell.* 165:1332–1345. <https://doi.org/10.1016/j.cell.2016.05.041>
- Kumar, P., L. Monin, P. Castillo, W. Elsegeiny, W. Horne, T. Eddens, A. Vikram, M. Good, A.A. Schoenborn, K. Bibby, et al. 2016. Intestinal interleukin-17 receptor signaling mediates reciprocal control of the gut microbiota and autoimmune inflammation. *Immunity.* 44:659–671. <https://doi.org/10.1016/j.immuni.2016.02.007>
- Lavoie, S., K.L. Conway, K.G. Lassen, H.B. Jijon, H. Pan, E. Chun, M. Michaud, J.K. Lang, C.A. Gallini Comeau, J.M. Dreyfuss, et al. 2019. The Crohn's disease polymorphism, *ATG16L1* T300A, alters the gut microbiota and enhances the local Th1/Th17 response. *eLife.* 8:e39982. <https://doi.org/10.7554/eLife.39982>
- Lee, J.S., C.M. Tato, B. Joyce-Shaikh, M.F. Gulen, C. Cayatte, Y. Chen, W.M. Blumenschein, M. Judo, G. Ayanoglu, T.K. McClanahan, et al. 2015. Interleukin-23-independent IL-17 production regulates intestinal epithelial permeability. *Immunity.* 43:727–738. <https://doi.org/10.1016/j.immuni.2015.09.003>
- Ley, R.E., M. Hamady, C. Lozupone, P.J. Turnbaugh, R.R. Ramey, J.S. Bircher, M.L. Schlegel, T.A. Tucker, M.D. Schrenzel, R. Knight, and J.I. Gordon. 2008. Evolution of mammals and their gut microbes. *Science.* 320: 1647–1651. <https://doi.org/10.1126/science.1155725>
- Liu, S., W. Zhao, P. Lan, and X. Mou. 2021. The microbiome in inflammatory bowel diseases: from pathogenesis to therapy. *Protein Cell.* 12:331–345. <https://doi.org/10.1007/s12328-020-00745-3>
- Lo Presti, A., F. Zorzi, F. Del Chierico, A. Altomare, S. Cocca, A. Avola, F. De Biasio, A. Russo, E. Cella, S. Reddel, et al. 2019. Fecal and mucosal microbiota profiling in irritable bowel syndrome and inflammatory bowel disease. *Front. Microbiol.* 10:1655. <https://doi.org/10.3389/fmicb.2019.01655>
- Lupp, C., M.L. Robertson, M.E. Wickham, I. Sekirov, O.L. Champion, E.C. Gaynor, and B.B. Finlay. 2007. Host-mediated inflammation disrupts the intestinal microbiota and promotes the overgrowth of Enterobacteriaceae. *Cell Host Microbe.* 2:119–129. <https://doi.org/10.1016/j.chom.2007.06.010>
- Mao, K., A.P. Baptista, S. Tamoutounour, L. Zhuang, N. Bouladoux, A.J. Martins, Y. Huang, M.Y. Gerner, Y. Belkaid, and R.N. Germain. 2018. Innate and adaptive lymphocytes sequentially shape the gut microbiota and lipid metabolism. *Nature.* 554:255–259. <https://doi.org/10.1038/nature25437>
- Marcobal, A., A.M. Southwick, K.A. Earle, and J.L. Sonnenburg. 2013. A refined palate: bacterial consumption of host glycans in the gut. *Glycobiology.* 23:1038–1046. <https://doi.org/10.1093/glycob/cwt040>
- Mariño, G., A.F. Fernández, S. Cabrera, Y.W. Lundberg, R. Cabanillas, F. Rodríguez, N. Salvador-Montoliu, J.A. Vega, A. Germanà, A. Fueyo, et al. 2010. Autophagy is essential for mouse sense of balance. *J. Clin. Invest.* 120:2331–2344. <https://doi.org/10.1172/JCI42601>
- Marsland, B.J., and E.S. Gollwitzer. 2014. Host-microorganism interactions in lung diseases. *Nat. Rev. Immunol.* 14:827–835. <https://doi.org/10.1038/nri3769>
- McGuckin, M.A., S.K. Lindén, P. Sutton, and T.H. Florin. 2011. Mucin dynamics and enteric pathogens. *Nat. Rev. Microbiol.* 9:265–278. <https://doi.org/10.1038/nrmicro2538>
- Miyoshi, M., M. Usami, and A. Ohata. 2008. Short-chain fatty acids and trichostatin A alter tight junction permeability in human umbilical vein endothelial cells. *Nutrition.* 24:1189–1198. <https://doi.org/10.1016/j.nut.2008.06.012>
- Nesta, B., M. Valeri, A. Spagnuolo, R. Rosini, M. Mora, P. Donato, C.J. Alteri, M. Del Vecchio, S. Buccato, A. Pezzicoli, et al. 2014. SSIe elicits functional antibodies that impair in vitro mucinase activity and in vivo colonization by both intestinal and extraintestinal *Escherichia coli* strains. *PLoS Pathog.* 10:e1004124. <https://doi.org/10.1371/journal.ppat.1004124>
- Newton, R.H., S. Shrestha, J.M. Sullivan, K.B. Yates, E.B. Compeer, N. Ron-Harel, B.R. Blazar, S.J. Bensinger, W.N. Haining, M.L. Dustin, et al. 2018. Maintenance of CD4 T cell fitness through regulation of Foxo1. *Nat. Immunol.* 19:838–848. <https://doi.org/10.1038/s41590-018-0157-4>
- Noah, T.K., B. Donahue, and N.F. Shroyer. 2011. Intestinal development and differentiation. *Exp. Cell Res.* 317:2702–2710. <https://doi.org/10.1016/j.yexcr.2011.09.006>
- Ohata, A., M. Usami, and M. Miyoshi. 2005. Short-chain fatty acids alter tight junction permeability in intestinal monolayer cells via lipoxygenase activation. *Nutrition.* 21:838–847. <https://doi.org/10.1016/j.nut.2004.12.004>
- Okumura, R., T. Kurakawa, T. Nakano, H. Kayama, M. Kinoshita, D. Motooka, K. Gotoh, T. Kimura, N. Kamiyama, T. Kusu, et al. 2016. Lypd8 promotes the segregation of flagellated microbiota and colonic epithelia. *Nature.* 532:117–121. <https://doi.org/10.1038/nature17406>
- Olszak, T., J.F. Neves, C.M. Dowds, K. Baker, J. Glickman, N.O. Davidson, C.S. Lin, C. Jobin, S. Brand, K. Sotlar, et al. 2014. Protective mucosal immunity mediated by epithelial CD1d and IL-10. *Nature.* 509:497–502. <https://doi.org/10.1038/nature13150>
- Ouyang, W., W. Liao, C.T. Luo, N. Yin, M. Huse, M.V. Kim, M. Peng, P. Chan, Q. Ma, Y. Mo, et al. 2012. Novel Foxo1-dependent transcriptional programs control T<sub>reg</sub> cell function. *Nature.* 491:554–559. <https://doi.org/10.1038/nature11581>
- Paik, J.H., R. Kollipara, G. Chu, H. Ji, Y. Xiao, Z. Ding, L. Miao, Z. Tothova, J.W. Horner, D.R. Carrasco, et al. 2007. FoxOs are lineage-restricted redundant tumor suppressors and regulate endothelial cell homeostasis. *Cell.* 128:309–323. <https://doi.org/10.1016/j.cell.2006.12.029>
- Patel, K.K., H. Miyoshi, W.L. Beatty, R.D. Head, N.P. Malvin, K. Cadwell, J.L. Guan, T. Saitoh, S. Akira, P.O. Seglen, et al. 2013. Autophagy proteins control goblet cell function by potentiating reactive oxygen species production. *EMBO J.* 32:3130–3144. <https://doi.org/10.1038/emboj.2013.233>
- Peng, L., Z.R. Li, R.S. Green, I.R. Holzman, and J. Lin. 2009. Butyrate enhances the intestinal barrier by facilitating tight junction assembly via activation of AMP-activated protein kinase in Caco-2 cell monolayers. *J. Nutr.* 139:1619–1625. <https://doi.org/10.3945/jn.109.104638>
- Perez-Lopez, A., J. Behnsen, S.P. Nuccio, and M. Raffatellu. 2016. Mucosal immunity to pathogenic intestinal bacteria. *Nat. Rev. Immunol.* 16: 135–148. <https://doi.org/10.1038/nri.2015.17>
- Peterson, L.W., and D. Artis. 2014. Intestinal epithelial cells: regulators of barrier function and immune homeostasis. *Nat. Rev. Immunol.* 14: 141–153. <https://doi.org/10.1038/nri3608>
- Pudlo, N.A., K. Urs, S.S. Kumar, J.B. German, D.A. Mills, and E.C. Martens. 2015. Symbiotic human gut bacteria with variable metabolic priorities for host mucosal glycans. *MBio.* 6:e01282–e15. <https://doi.org/10.1128/mBio.01282-15>
- Rawls, J.F., M.A. Mahowald, R.E. Ley, and J.I. Gordon. 2006. Reciprocal gut microbiota transplants from zebrafish and mice to germ-free recipients reveal host habitat selection. *Cell.* 127:423–433. <https://doi.org/10.1016/j.cell.2006.08.043>
- Salem, F., N. Kindt, J.R. Marchesi, P. Netter, A. Lopez, T. Kokten, S. Danese, J.Y. Jouzeau, L. Peyrin-Biroulet, and D. Moulin. 2019. Gut microbiome in chronic rheumatic and inflammatory bowel diseases: Similarities and differences. *United European Gastroenterol. J.* 7:1008–1032. <https://doi.org/10.1177/2050640619867555>
- Sato, T., R.G. Vries, H.J. Snippert, M. van de Wetering, N. Barker, D.E. Stange, J.H. van Es, A. Abo, P. Kujala, P.J. Peters, and H. Clevers. 2009. Single Lgr5 stem cells build crypt-villus structures in vitro without a mesenchymal niche. *Nature.* 459:262–265. <https://doi.org/10.1038/nature07935>
- Segata, N., J. Izard, L. Waldron, D. Gevers, L. Miropolsky, W.S. Garrett, and C. Huttenhower. 2011. Metagenomic biomarker discovery and explanation. *Genome Biol.* 12:R60. <https://doi.org/10.1186/gb-2011-12-6-r60>
- Shan, M., M. Gentile, J.R. Yeiser, A.C. Walland, V.U. Bornstein, K. Chen, B. He, L. Cassia, A. Bigas, M. Cols, et al. 2013. Mucus enhances gut homeostasis and oral tolerance by delivering immunoregulatory signals. *Science.* 342: 447–453. <https://doi.org/10.1126/science.1237910>
- Snoeks, L., C.R. Weber, K. Wasland, J.R. Turner, C. Vainder, W. Qi, and S.D. Savkovic. 2009. Tumor suppressor FOXO3 participates in the regulation of intestinal inflammation. *Lab. Invest.* 89:1053–1062. <https://doi.org/10.1038/labinvest.2009.66>
- Specian, R.D., and M.G. Oliver. 1991. Functional biology of intestinal goblet cells. *Am. J. Physiol.* 260:C183–C193. <https://doi.org/10.1152/ajpcell.1991.260.2.C183>

- Sun, M., W. Wu, L. Chen, W. Yang, X. Huang, C. Ma, F. Chen, Y. Xiao, Y. Zhao, C. Ma, et al. 2018. Microbiota-derived short-chain fatty acids promote Th1 cell IL-10 production to maintain intestinal homeostasis. *Nat. Commun.* 9:3555. <https://doi.org/10.1038/s41467-018-05901-2>
- Sun, M., Y. Shinoda, and K. Fukunaga. 2019a. KY-226 protects blood-brain barrier function through the Akt/FoxO1 signaling pathway in brain ischemia. *Neuroscience*. 399:89–102. <https://doi.org/10.1016/j.neuroscience.2018.12.024>
- Sun, Z., W. Pei, Y. Guo, Z. Wang, R. Shi, X. Chen, X. Zhao, C. Chen, J. Liu, X. Tan, et al. 2019b. Gut microbiota-mediated NLRP12 expression drives the attenuation of dextran sulphate sodium-induced ulcerative colitis by Qingchang Wenzhong Decoction. *Evid. Based Complement. Alternat. Med.* 2019:9839474. <https://doi.org/10.1155/2019/9839474>
- Taddei, A., C. Giampietro, A. Conti, F. Orsenigo, F. Breviario, V. Pirazzoli, M. Potente, C. Daly, S. Dimmeler, and E. Dejana. 2008. Endothelial adherens junctions control tight junctions by VE-cadherin-mediated upregulation of claudin-5. *Nat. Cell Biol.* 10:923–934. <https://doi.org/10.1038/ncb1752>
- Turner, J.R. 2009. Intestinal mucosal barrier function in health and disease. *Nat. Rev. Immunol.* 9:799–809. <https://doi.org/10.1038/nri2653>
- Tytgat, K.M., H.A. Büller, F.J. Opdam, Y.S. Kim, A.W. Einerhand, and J. Dekker. 1994. Biosynthesis of human colonic mucin: Muc2 is the prominent secretory mucin. *Gastroenterology*. 107:1352–1363. [https://doi.org/10.1016/0016-5085\(94\)90537-1](https://doi.org/10.1016/0016-5085(94)90537-1)
- Ushio, H., T. Ueno, Y. Kojima, M. Komatsu, S. Tanaka, A. Yamamoto, Y. Ichimura, J. Ezaki, K. Nishida, S. Komazawa-Sakon, et al. 2011. Crucial role for autophagy in degranulation of mast cells. *J. Allergy Clin. Immunol.* 127:1267–76.e6. <https://doi.org/10.1016/j.jaci.2010.12.1078>
- Vaishnavi, S., M. Yamamoto, K.M. Severson, K.A. Ruhn, X. Yu, O. Koren, R. Ley, E.K. Wakeland, and L.V. Hooper. 2011. The antibacterial lectin RegIIIgamma promotes the spatial segregation of microbiota and host in the intestine. *Science*. 334:255–258. <https://doi.org/10.1126/science.1209791>
- van der Horst, A., and B.M. Burgering. 2007. Stressing the role of FoxO proteins in lifespan and disease. *Nat. Rev. Mol. Cell Biol.* 8:440–450. <https://doi.org/10.1038/nrm2190>
- Van der Sluis, M., B.A. De Koning, A.C. De Bruijn, A. Velcich, J.P. Meijerink, J.B. Van Goudoever, H.A. Büller, J. Dekker, I. Van Seuning, I.B. Renes, and A.W. Einerhand. 2006. Muc2-deficient mice spontaneously develop colitis, indicating that MUC2 is critical for colonic protection. *Gastroenterology*. 131:117–129. <https://doi.org/10.1053/j.gastro.2006.04.020>
- van der Vos, K.E., and P.J. Coffey. 2012. Glutamine metabolism links growth factor signaling to the regulation of autophagy. *Autophagy*. 8:1862–1864. <https://doi.org/10.4161/auto.22152>
- Vester-Andersen, M.K., H.C. Mirsepasi-Lauridsen, M.V. Prossberg, C.O. Mortensen, C. Träger, K. Skovsen, T. Thorkilgaard, C. Nøjgaard, I. Vind, K.A. Kroghfelt, et al. 2019. Increased abundance of proteobacteria in aggressive Crohn's disease seven years after diagnosis. *Sci. Rep.* 9:13473. <https://doi.org/10.1038/s41598-019-49833-3>
- Waldecker, M., T. Kautenburger, H. Daumann, C. Busch, and D. Schrenk. 2008. Inhibition of histone-deacetylase activity by short-chain fatty acids and some polyphenol metabolites formed in the colon. *J. Nutr. Biochem.* 19:587–593. <https://doi.org/10.1016/j.jnutbio.2007.08.002>
- Wang, H.B., P.Y. Wang, X. Wang, Y.L. Wan, and Y.C. Liu. 2012. Butyrate enhances intestinal epithelial barrier function via up-regulation of tight junction protein Claudin-1 transcription. *Dig. Dis. Sci.* 57:3126–3135. <https://doi.org/10.1007/s10620-012-2259-4>
- Wang, K., M. Liao, N. Zhou, L. Bao, K. Ma, Z. Zheng, Y. Wang, C. Liu, W. Wang, J. Wang, et al. 2019. *Parabacteroides distasonis* alleviates obesity and metabolic dysfunctions via production of succinate and secondary bile acids. *Cell Rep.* 26:222–235.e5. <https://doi.org/10.1016/j.celrep.2018.12.028>
- Wilhelm, K., K. Happel, G. Eelen, S. Schoors, M.F. Oellerich, R. Lim, B. Zimmermann, I.M. Aspalter, C.A. Franco, T. Boettger, et al. 2016. FOXO1 couples metabolic activity and growth state in the vascular endothelium. *Nature*. 529:216–220. <https://doi.org/10.1038/nature16498>
- Willemsen, L.E., M.A. Koetsier, S.J. van Deventer, and E.A. van Tol. 2003. Short chain fatty acids stimulate epithelial mucin 2 expression through differential effects on prostaglandin E<sub>1</sub> and E<sub>2</sub> production by intestinal myofibroblasts. *Gut*. 52:1442–1447. <https://doi.org/10.1136/gut.52.10.1442>
- Wlodarska, M., C.A. Thaiss, R. Nowarski, J. Henao-Mejia, J.P. Zhang, E.M. Brown, G. Frankel, M. Levy, M.N. Katz, W.M. Philbrick, et al. 2014. NLRP6 inflammasome orchestrates the colonic host-microbial interface by regulating goblet cell mucus secretion. *Cell*. 156:1045–1059. <https://doi.org/10.1016/j.cell.2014.01.026>
- Wright, D.P., D.I. Rosendale, and A.M. Robertson. 2000. Prevotella enzymes involved in mucin oligosaccharide degradation and evidence for a small operon of genes expressed during growth on mucin. *FEMS Microbiol. Lett.* 190:73–79. <https://doi.org/10.1111/j.1574-6968.2000.tb09265.x>
- Wu, C., Z. Chen, S. Xiao, T. Thalhamer, A. Madi, T. Han, and V. Kuchroo. 2018a. SGK1 governs the reciprocal development of Th17 and regulatory T cells. *Cell Rep.* 22:653–665. <https://doi.org/10.1016/j.celrep.2017.12.068>
- Wu, M., Y. Wu, J. Li, Y. Bao, Y. Guo, and W. Yang. 2018b. The dynamic changes of gut microbiota in Muc2 deficient mice. *Int. J. Mol. Sci.* 19:2809. <https://doi.org/10.3390/ijms19092809>
- Zhang, L., J. Li, L.H. Young, and M.J. Caplan. 2006. AMP-activated protein kinase regulates the assembly of epithelial tight junctions. *Proc. Natl. Acad. Sci. USA*. 103:17272–17277. <https://doi.org/10.1073/pnas.0608531103>
- Zhao, Y., J. Yang, W. Liao, X. Liu, H. Zhang, S. Wang, D. Wang, J. Feng, L. Yu, and W.G. Zhu. 2010. Cytosolic FoxO1 is essential for the induction of autophagy and tumour suppressor activity. *Nat. Cell Biol.* 12:665–675. <https://doi.org/10.1038/ncb2069>
- Zheng, L., C.J. Kelly, K.D. Battista, R. Schaefer, J.M. Lanis, E.E. Alexeev, R.X. Wang, J.C. Onyiah, D.J. Kominsky, and S.P. Colgan. 2017. Microbial-derived butyrate promotes epithelial barrier function through IL-10 receptor-dependent repression of claudin-2. *J. Immunol.* 199:2976–2984. <https://doi.org/10.4049/jimmunol.1700105>
- Zhong, Y., M. Nyman, and F. Fåk. 2015. Modulation of gut microbiota in rats fed high-fat diets by processing whole-grain barley to barley malt. *Mol. Nutr. Food Res.* 59:2066–2076. <https://doi.org/10.1002/mnfr.201500187>
- Zhou, W., Q. Cao, Y. Peng, Q.J. Zhang, D.H. Castrillon, R.A. DePinho, and Z.P. Liu. 2009. FoxO4 inhibits NF-kappaB and protects mice against colonic injury and inflammation. *Gastroenterology*. 137:1403–1414. <https://doi.org/10.1053/j.gastro.2009.06.049>

Supplemental material

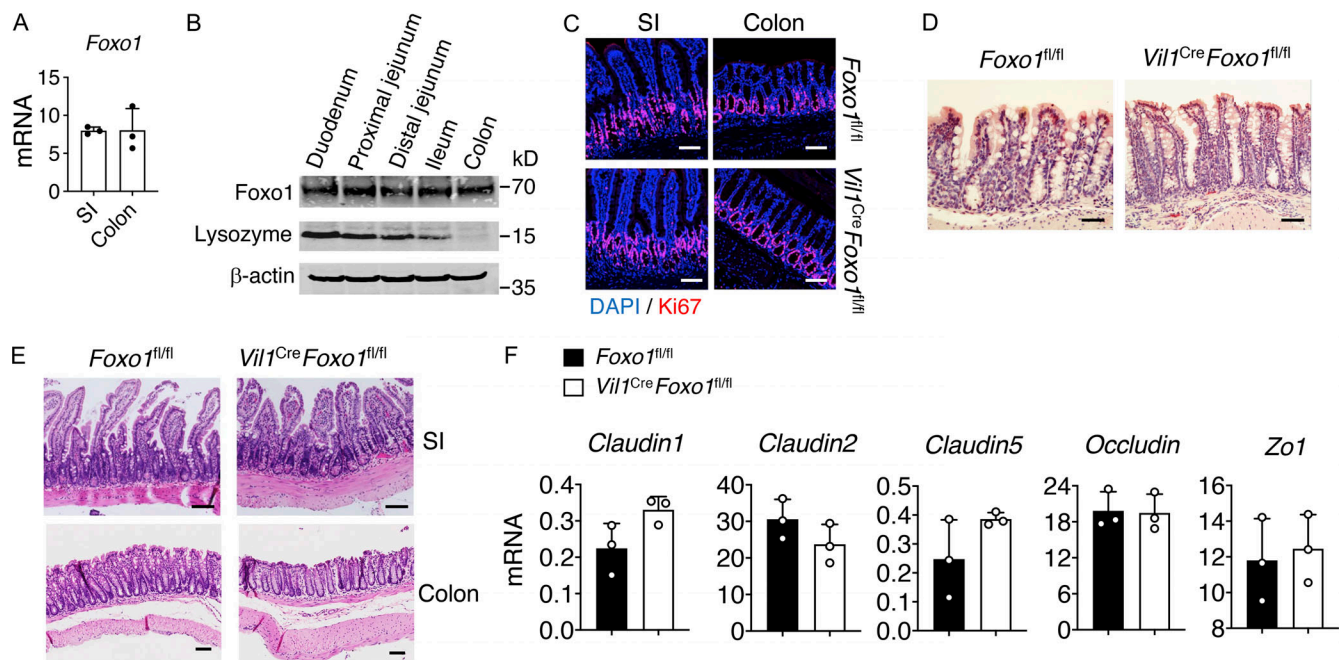
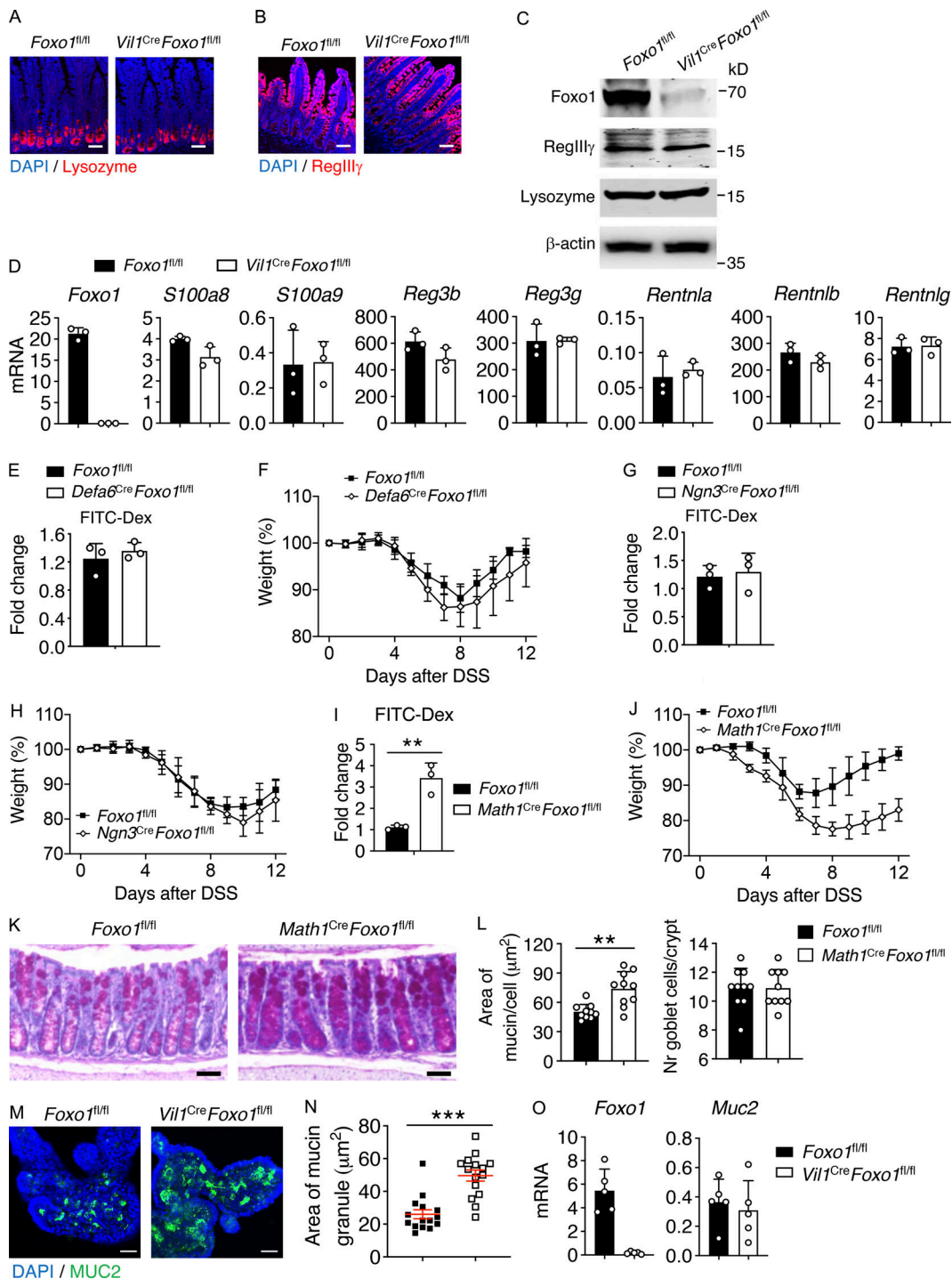


Figure S1. **Foxo1 does not affect IEC proliferation and apoptosis.** (A) mRNA level of *Foxo1* from small intestine (SI) and colon IECs of WT mice under steady state. (B) Immunoblot analysis of *Foxo1*, lysozyme, and  $\beta$ -actin in IECs from the indicated compartments of the intestines from WT mice under steady state. (C) Ki-67 (red) and DAPI (blue) staining of colons from *Foxo1<sup>fl/fl</sup>* and *Vil1<sup>Cre</sup>Foxo1<sup>fl/fl</sup>* mice. Scale bar, 50  $\mu$ m. (D) Terminal deoxynucleotidyl transferase dUTP nick end labeling staining of the colonic tissues. No difference was found between *Foxo1<sup>fl/fl</sup>* and *Vil1<sup>Cre</sup>Foxo1<sup>fl/fl</sup>* mice. Scale bar, 100  $\mu$ m. (E) H&E staining of the SI and colon from 8-wk-old *Foxo1<sup>fl/fl</sup>* and *Vil1<sup>Cre</sup>Foxo1<sup>fl/fl</sup>* mice. Scale bar, 100  $\mu$ m. (F) mRNA level of indicated TJ genes from IECs of *Foxo1<sup>fl/fl</sup>* and *Vil1<sup>Cre</sup>Foxo1<sup>fl/fl</sup>* mice. Data are representative of three independent experiments (A-F).



**Figure S2. Foxo1 deficiency in goblet cells impairs intestinal barrier integrity.** (A) Lysozyme (red) and DAPI (blue) staining of the small intestine (SI) from 8-wk-old *Foxo1<sup>fl/fl</sup>* and *Vil1<sup>Cre</sup>Foxo1<sup>fl/fl</sup>* mice. Scale bar, 50 μm. (B) RegIIIγ (red) and DAPI (blue) staining of SI from 8-wk-old *Foxo1<sup>fl/fl</sup>* and *Vil1<sup>Cre</sup>Foxo1<sup>fl/fl</sup>* mice. Scale bar, 50 μm. (C) Immunoblot analysis of Foxo1, RegIIIγ, lysozyme, and β-actin in IECs from the SI of 8-wk-old *Foxo1<sup>fl/fl</sup>* and *Vil1<sup>Cre</sup>Foxo1<sup>fl/fl</sup>* mice. (D) qPCR analysis of the indicated genes in IECs isolated from the SI of WT and *Foxo1<sup>ΔIEC</sup>* mice. (E) Intestinal barrier permeability was assessed by FITC-dextran assays between *Foxo1<sup>fl/fl</sup>* and *Defa6<sup>Cre</sup>Foxo1<sup>fl/fl</sup>* mice. (F) Body weights of *Foxo1<sup>fl/fl</sup>* and *Defa6<sup>Cre</sup>Foxo1<sup>fl/fl</sup>* mice during DSS-induced colitis. (G) Intestinal barrier permeability was assessed by FITC-dextran assays between *Foxo1<sup>fl/fl</sup>* and *Ngn3<sup>Cre</sup>Foxo1<sup>fl/fl</sup>* mice. (H) Body weights of *Foxo1<sup>fl/fl</sup>* and *Ngn3<sup>Cre</sup>Foxo1<sup>fl/fl</sup>* mice during DSS-induced colitis. (I) Intestinal barrier permeability was assessed by FITC-dextran (FITC-Dex) assays between *Foxo1<sup>fl/fl</sup>* and *Math1<sup>Cre</sup>Foxo1<sup>fl/fl</sup>* mice. (J) Body weights of *Foxo1<sup>fl/fl</sup>* and *Math1<sup>Cre</sup>Foxo1<sup>fl/fl</sup>* mice during DSS-induced colitis. (K) PAS staining of colons from 8-wk-old *Foxo1<sup>fl/fl</sup>* and *Math1<sup>Cre</sup>Foxo1<sup>fl/fl</sup>* mice. Scale bar, 100 μm. (L) Quantification of average mucin area/goblet cell (left) and of the average number of goblet cells per crypt (right) in *Foxo1<sup>fl/fl</sup>* and *Math1<sup>Cre</sup>Foxo1<sup>fl/fl</sup>* mice. >100 crypts were measured per mouse. (M–O) Goblet cell-enriched intestinal organoids were generated from *Foxo1<sup>fl/fl</sup>* and *Vil1<sup>Cre</sup>Foxo1<sup>fl/fl</sup>* mice. (M) Representative immunofluorescence staining for MUC2 and DAPI is shown. Scale bar, 20 μm. (N) Quantification of mucin granule area. (O) qPCR analysis of indicated genes in organoids. Data are representative of three independent experiments (A–E, G, I, K, and M) or are pooled from two independent experiments (F, H, J, L, N, and O). \*\*, P < 0.01; \*\*\*, P < 0.001 (Student's *t* test; error bars represent SD).

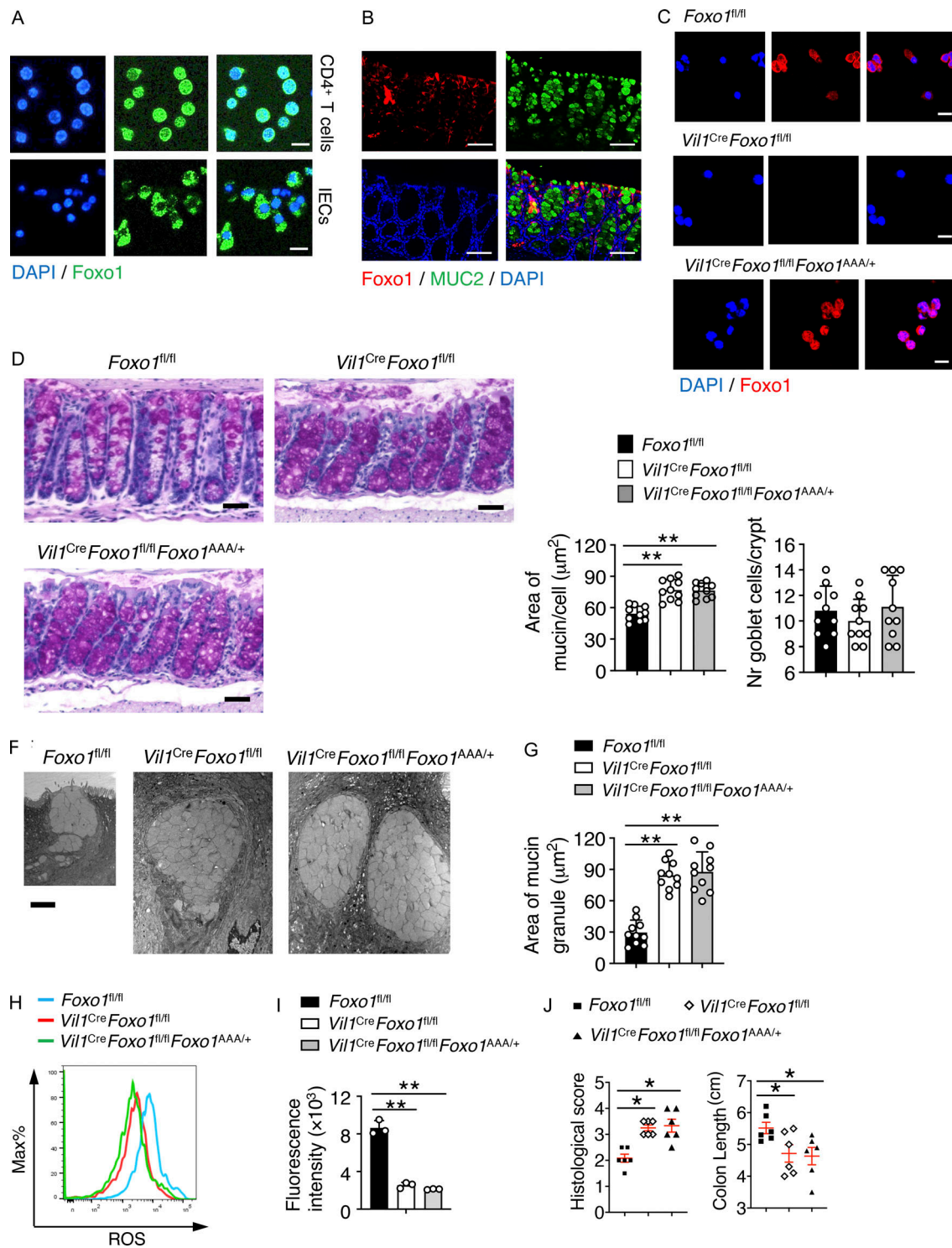
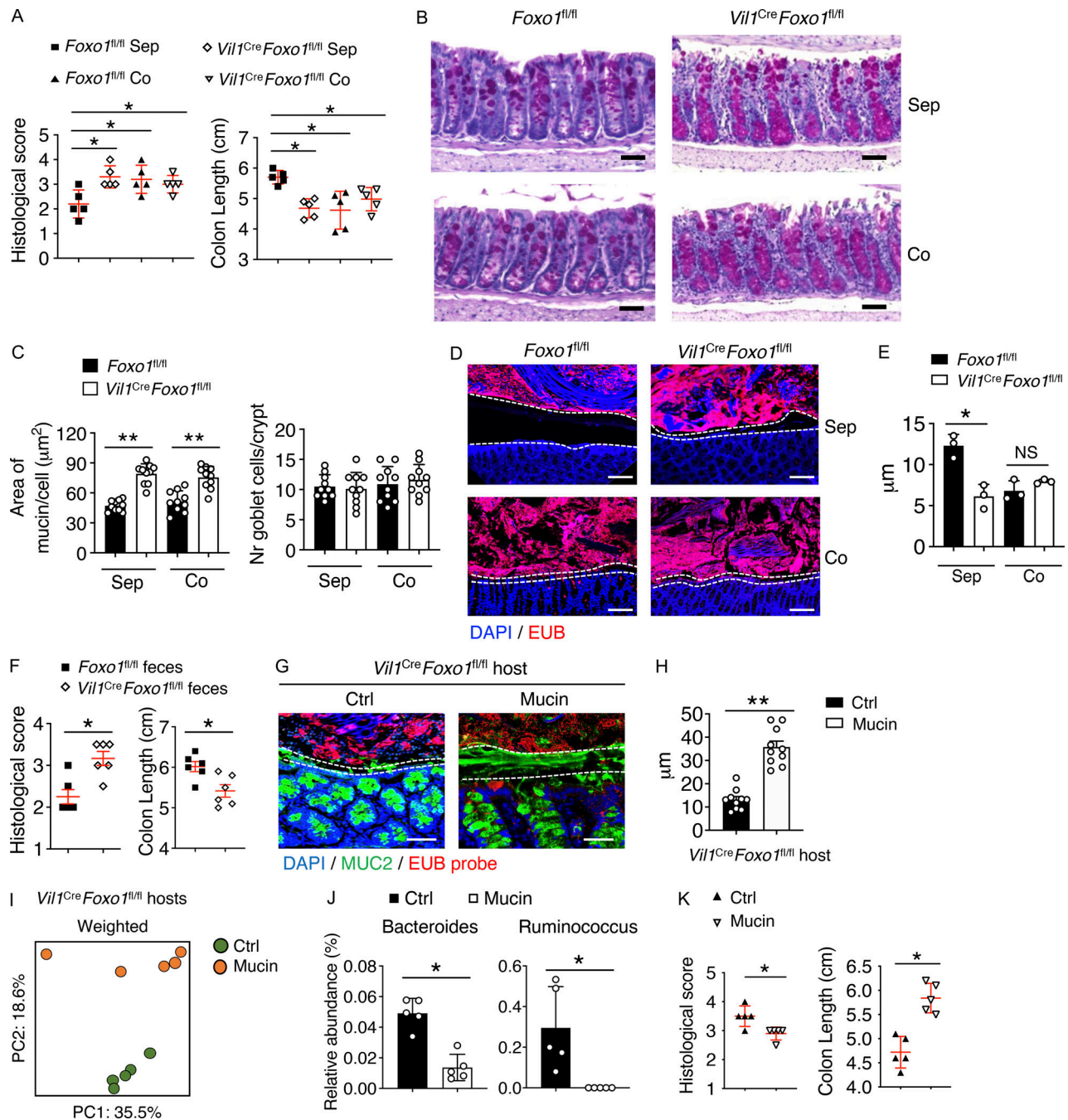


Figure S3. **Cytosolic Foxo1 regulates goblet cell autophagy.** (A) Foxo1 (green) and DAPI (blue) staining of WT splenic CD4<sup>+</sup> T cells and colonic IECs. Scale bar, 500 μm. (B) MUC2 (green) and Foxo1 (red) with DAPI (blue) staining of colonic tissue from WT mice. Scale bar, 50 μm. (C) Foxo1 (red) and DAPI (blue) staining of colonic IECs from *Foxo1<sup>fl/fl</sup>*, *Vil1<sup>Cre</sup>Foxo1<sup>fl/fl</sup>*, and *Vil1<sup>Cre</sup>Foxo1<sup>fl/fl</sup>Foxo1<sup>AAA/+</sup>* mice. Scale bar, 500 μm. (D) PAS staining of colons from 8-wk-old *Foxo1<sup>fl/fl</sup>*, *Vil1<sup>Cre</sup>Foxo1<sup>fl/fl</sup>*, and *Vil1<sup>Cre</sup>Foxo1<sup>fl/fl</sup>Foxo1<sup>AAA/+</sup>* mice. Scale bar, 50 μm. (E) Quantification of average mucin area/goblet cell (left) and of the average number of goblet cells per crypt (right) in *Foxo1<sup>fl/fl</sup>*, *Vil1<sup>Cre</sup>Foxo1<sup>fl/fl</sup>*, and *Vil1<sup>Cre</sup>Foxo1<sup>fl/fl</sup>Foxo1<sup>AAA/+</sup>* mice from D (>100 crypts were measured per mouse). (F) TEM images of upper crypt goblet cells from *Foxo1<sup>fl/fl</sup>*, *Vil1<sup>Cre</sup>Foxo1<sup>fl/fl</sup>*, and *Vil1<sup>Cre</sup>Foxo1<sup>fl/fl</sup>Foxo1<sup>AAA/+</sup>* murine colons. Scale bar, 2 μm. (G) Quantification of average mucin granule area from F. (H) Expression of ROS (DCFDA) on *Foxo1<sup>fl/fl</sup>*, *Vil1<sup>Cre</sup>Foxo1<sup>fl/fl</sup>*, and *Vil1<sup>Cre</sup>Foxo1<sup>fl/fl</sup>Foxo1<sup>AAA/+</sup>* colonic IECs assessed by flow cytometry. (I) Expression of ROS (DCFDA) on *Foxo1<sup>fl/fl</sup>*, *Vil1<sup>Cre</sup>Foxo1<sup>fl/fl</sup>*, and *Vil1<sup>Cre</sup>Foxo1<sup>fl/fl</sup>Foxo1<sup>AAA/+</sup>* colonic IECs assessed by fluorescent plate reader. (J) Histological score (left) and colon lengths (right) of *Foxo1<sup>fl/fl</sup>*, *Vil1<sup>Cre</sup>Foxo1<sup>fl/fl</sup>*, and *Vil1<sup>Cre</sup>Foxo1<sup>fl/fl</sup>Foxo1<sup>AAA/+</sup>* mice during DSS-induced colitis as in Fig. 3 L, measured from the colocolic junction to the anal verge. Data are representative of three independent experiments (A–D, F, H, and I) or are pooled from two independent experiments (E, G, and J). \*, P < 0.05; \*\*, P < 0.01 (Student's *t* test; error bars represent SD).



**Figure S4. IEC-derived Foxo1 governs bidirectional regulation of mucus and gut microbiota.** (A) Histological score (left) and colon lengths (right) of *Foxo1<sup>fl/fl</sup>* and *Vil1<sup>Cre</sup>Foxo1<sup>fl/fl</sup>* mice under either separated (Sep) housing or cohousing (Co) conditions during DSS-induced colitis as in Fig. 4 B, measured from the colocecal junction to the anal verge. (B) PAS staining of the colons from 8-wk-old *Foxo1<sup>fl/fl</sup>* and *Vil1<sup>Cre</sup>Foxo1<sup>fl/fl</sup>* mice under either separated housing or cohousing conditions. Scale bar, 100  $\mu\text{m}$ . (C) Quantification of average mucin area/goblet cell in *Foxo1<sup>fl/fl</sup>* and *Vil1<sup>Cre</sup>Foxo1<sup>fl/fl</sup>* mice (left) and of the average number of goblet cells per crypt (right) under either separated housing or cohousing conditions from B (>100 crypts were measured per mouse). (D) Hybridization of EUB338 probe (red) and DAPI (blue) in the colons from *Foxo1<sup>fl/fl</sup>* and *Vil1<sup>Cre</sup>Foxo1<sup>fl/fl</sup>* mice under either separated housing or cohousing conditions. The white dash represents the distance between bacteria and colonic tissue. Scale bar, 100  $\mu\text{m}$ . (E) Quantification of segregation distance in the colons from *Foxo1<sup>fl/fl</sup>* and *Vil1<sup>Cre</sup>Foxo1<sup>fl/fl</sup>* mice under either separated housing or cohousing conditions from D (>10 fields were measured per mouse). (F) Histological score (left) and colon lengths (right) of GF WT mice with *Foxo1<sup>fl/fl</sup>* or *Vil1<sup>Cre</sup>Foxo1<sup>fl/fl</sup>* fecal transplant as in Fig. 5 E, measured from the colocecal junction to the anal verge. (G) Representative immunofluorescence staining for mucus using MUC2 (green) and EUB338 probe (red) with DAPI (blue) in *Vil1<sup>Cre</sup>Foxo1<sup>fl/fl</sup>* mice with mucin reconstitution. The white dashed lines outline the inner mucus layer. Scale bar, 50  $\mu\text{m}$ . (H) Quantification of inner mucus layer thickness in the colon in *Vil1<sup>Cre</sup>Foxo1<sup>fl/fl</sup>* mice as in Fig. S4 G (>10 fields were measured per mouse). (I) Principal coordinate (PC) analysis of weighted unique fraction metric distances for 16S rDNA of the fecal bacteria composition from *Vil1<sup>Cre</sup>Foxo1<sup>fl/fl</sup>* host mice with or without mucin treatment. (J) Relative abundance of indicated bacterial genera in fecal samples from different groups. (K) Histological score (left) and colon lengths (right) of *Vil1<sup>Cre</sup>Foxo1<sup>fl/fl</sup>* mice as in Fig. 5 I, measured from the colocecal junction to the anal verge. Data are representative of three independent experiments (B, D, G, I, and J) or are pooled from at least two independent experiments (A, C, E, F, H, and K). \*,  $P < 0.05$ ; \*\*,  $P < 0.01$  (Student's *t* test; error bars represent SD).

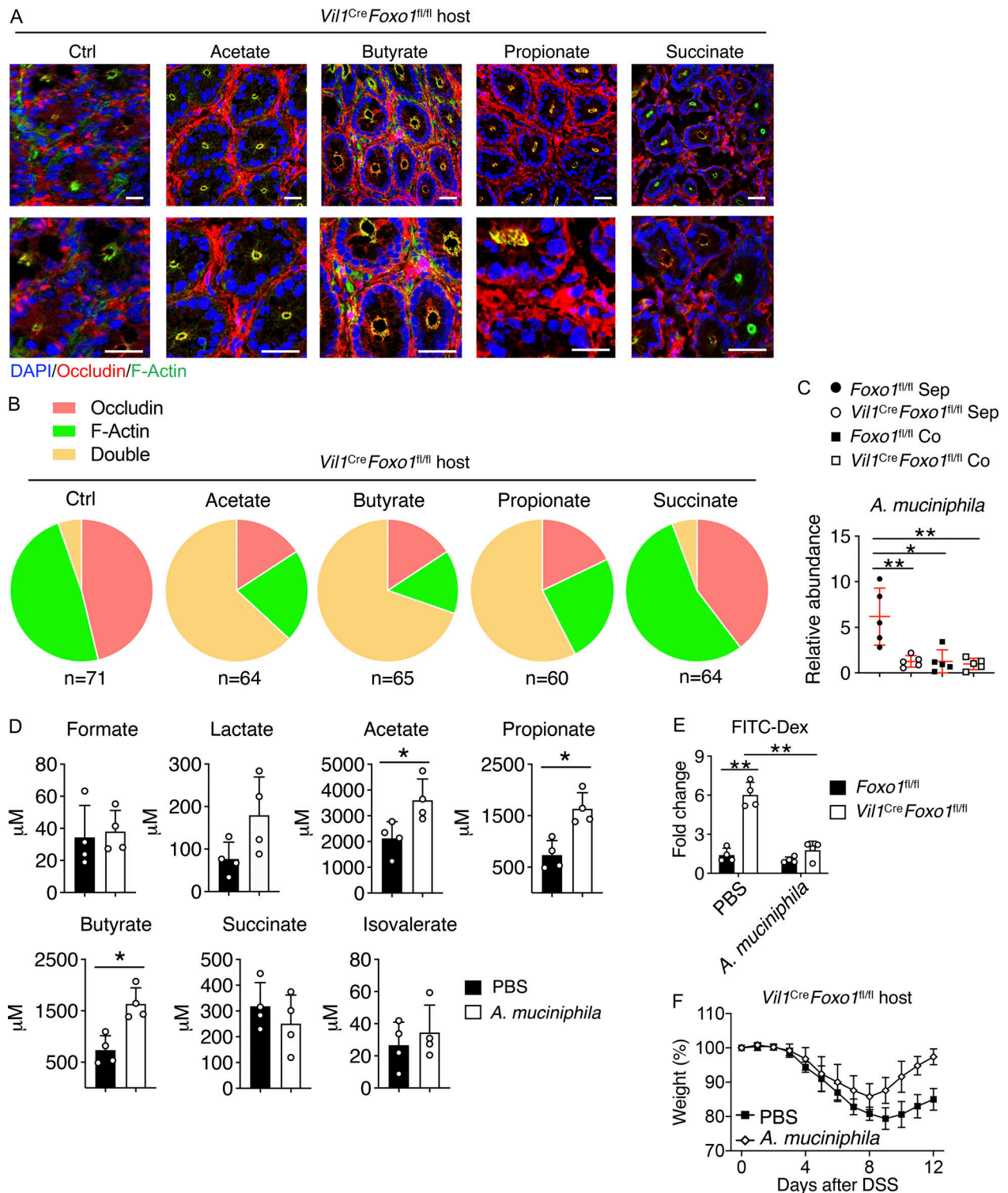


Figure S5. **IEC-derived Foxo1 maintains epithelial TJs through bacterial SCFA metabolism.** **(A)** Representative immunofluorescence staining for mucus using occludin (red) and F-actin (green) with DAPI (blue) in the colons of *Vil1<sup>Cre</sup>Foxo1<sup>fl/fl</sup>* mice with the indicated treatment. The lower row represents a magnified image from the upper row. Scale bar, 15  $\mu$ m. **(B)** Quantitative analysis of occludin colocalization with F-actin in colonic IECs as in A. Occludin, occluding-positive cells, no colocalization; F-actin, F-actin single-positive cells, no colocalization; Double, occludin and F-actin double-positive cells. **(C)** The abundance of *A. muciniphila* in fecal samples from different groups was analyzed by qPCR. **(D)** Quantification of indicated SCFAs from the feces of *Vil1<sup>Cre</sup>Foxo1<sup>fl/fl</sup>* mice with *A. muciniphila* treatment or control PBS. **(E and F)** *A. muciniphila* was administered to the mice by oral gavage every day for 2 wk before further examination. **(E)** Intestinal barrier permeability was assessed by FITC-dextran assay between *Foxo1<sup>fl/fl</sup>* and *Vil1<sup>Cre</sup>Foxo1<sup>fl/fl</sup>* mice. **(F)** Body weights of *Vil1<sup>Cre</sup>Foxo1<sup>fl/fl</sup>* mice with the indicated treatment during DSS-induced colitis. The mice were given *A. muciniphila* for another 1 wk when DSS treatment started. Data are representative of two independent experiments (A, C, and D) or are pooled from two independent experiments (B, E, and F). \*,  $P < 0.05$ ; \*\*,  $P < 0.01$  (Student's  $t$  test; error bars represent SD).